SCIENCE OF LIGHT

VOLUME 3 NUMBER 1

August
1954

Published by the

Institute for Optical Research

Tokyo University of Education

in collaboration with the

Spectroscopical Society of Japan

SCIENCE OF LIGHT

Science of Light contains reports of the Institute for Optical Research and contributions from other science bodies about similar subject.

All communications should be addressed to the director or to the librarian of the Institute.

The Institute for Optical Research

Tokyo University of Education

400, 4-chome, Hyakunin-machi, Sinjuku-ku, Tokyo, Japan

Printed by
Kokusai Bunken Insatsusha
Chiyoda-ku, Tokyo.

Obituary Notice of
TOSHIO KITAYAMA

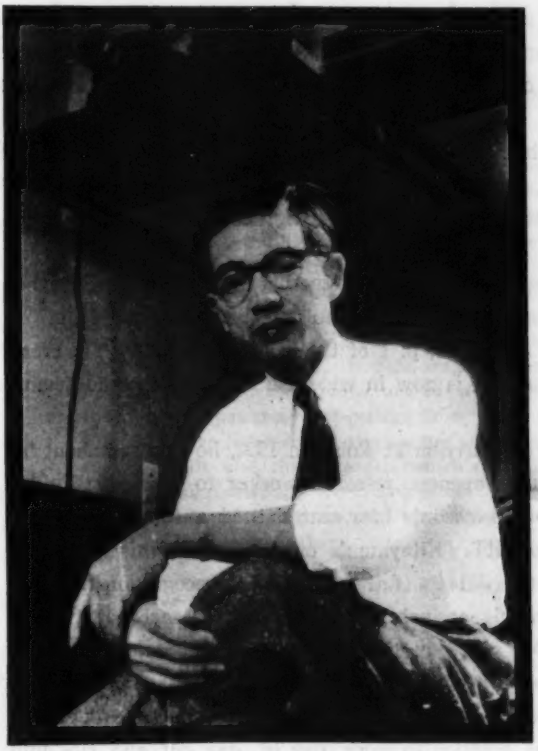

On September the 7th 1953, I received a cable from Professor George R. Harrison of the Massachusetts Institute of Technology, imparting the sorrowful news of the very unexpected passing of Toshio Kitayama, who had been engaged in studies in spectroscopy under Professor Harrison since the end of 1952. The message read: "Great regret to inform you of death from heart failure of Toshio Kitayama on September 7 at 2.20 p.m. Please inform family ....."

Toshio Kitayama was born at Wakayama, Japan, in 1913. In 1942 he graduated from the Tokyo University for Literature and Science (the predecessor of the Tokyo University of Education), and set out forthwith on the difficult task of ruling diffraction gratings. I myself collaborated in this work that took place in the Institute of Physical and Chemical Research, later reorganized as the Scientific Research Institute.

Work on gratings had been initiated in Japan by the late Prof. Nagaoka about twenty years earlier, but was then laid aside a couple of years later, to be left untouched until resumed by us in 1942. This was in the very midst of the Second World War: it was a time when almost all and every equipment and material was requisitioned and every factory mobilized for the war effort; and the shadow of enlistment was hanging over every man of age: certainly a most unfavourable time for anyone to be engaged in such unwarlike work as the ruling of gratings! Kitayama devoted himself wholly to the work, conquering

every obstacle that lay across his path. But the situation in Japan became increasingly critical, and from early 1945 the city of Tokyo was exposed to increasingly frequent and devastating air raids. Kitayama evacuated into the country with his colleagues and his instruments—first to Kanazawa, a city on the coast of the Sea of Japan,—then as this town also was thought menaced, further on to a tiny village on the seashore, where the end of the war found him and his group.

Then Kitayama's work had to be recommenced almost from the beginning: part of his ruling machine, left behind in Tokyo was irretrievably lost; all the equipment had to be readjusted: this meant retracing about three years of toil and work.

And yet Kitayama's indomitable and persevering spirit finally triumphed and his efforts crystallized in the first grating to be completed in Japan. A record of this work appears in Vol. 2, p. 1 of the Science of Light. The cross-ruled piece developed by Kitayama is now in wide use in Japan for the testing of electron micrscopes.

When I met Prof. George Harrison at Rome in 1952, he told me about his project of inviting some young Japanese research worker to take part in his work on spectroscopy. Prof. Harrison's idea materialized a few months later with Kitayama going over to MIT. Kitayama's enthusiasm for his work and his ability based on experience did not fail to win early recognition from his professor. Two weeks after his arrival in Cambridge, Massachusetts, Prof. Harrison wrote to me; "Our work in the Spectroscopy Laboratory is going forward very well, and we are very happy indeed to have Mr. Kitayama with us. He is a very able and conscientious worker and is making very good progress."

Unfortunately, his zealous devotion to work, day in, day out and late into the night must have little favoured his health. On the 7th of September, he was working in the laboratory as usual, Sunday notwithstanding. Two of his friends called on him and found him lying on a sofa, complaining that he felt a little sick. After a few words of conversation one of the visitors left the room. It was during the few moments following this that Kitayama passed away, to return no more.

I cannot find adequate words to express my regret for the loss of such a young and promising scientist when he was just on the threshold of his major work. I do believe however that his spirit will live forever amongst us to encourage and guide us with his unfaltering example.

April 15, 1954

Yoshio Fujioka

Theory of Grating with Circular Grooves (Curved grating)

Yoshimi SAKAYANAGI

Institute for Optical Research, Tokyo University of Education

(Received Nov. 5, 1953)

A curved grating is defined as one which has equidistant circular grooves ruled upon a concave mirror. In this paper an attempt has been made to develop the theory of the curved grating based on Beutler's paper, i.e. using the light path function. We will discuss the condition for eliminating astigmatism, the broadening of a spectral line due to the curved grooves, the amount of coma, etc. If the radius of curvature of the curved grooves is larger than twice the radius of the spherical mirror, i.e. if α_0 is less than 30°, there is a rather wide range in which astigmatism is very small. In this range, the broadening of a spectral line due to the curved groove, and coma also is small, which prevents the resolving power of the grating from being reduction. But outside this range the increase of astigmatism affects not only the length of the lines but also their breadth, which further is accompanied by decrease of the resolving power. Therefore this grating can be used only for a definite mounting, and not applicable to wide uses, as for instance with the Pashen mounting.

1. Introduction

Since the first production of the concave grating by Rowland[1], this instrument has been widely used for the study of spectroscopy. This is of course due to its many superior advantages as compared with other instruments, among which the most characteristic is its self-focusing property. However, the concave grating also has an inherent defect which stems from this very merit; namely the large astigmatism of the spectral lines.

The early days of spectroscopy, when the main problem was the determination of the wavelengths of spectra, this defect did not seem to be very serious. It was even regarded to some extent as an advantage, and we see Rowland stating in his book[1]: " it adds to the beauty of the spectra, as the horizontal lines due to dust in the slit are never present, as dust has a different focal length from the lines of the spectrum".

With the advance of spectroscopy, the measurement of the intensities of spectral lines has become quite as important as that of the wave-lengths. For this purpose, of course with the concurrence of the development of techniques

1) H. A. Rowland: Phil. Mag. (4) XIII (1882) 469.

in general, it has become necessary to use other instruments in conjunction with the concave grating. For instance an optical wedge is used for intensity measurement, and the crossing interferometer applied for the measurement of hyper fine structures. And these methods are applicable only for stigmatic spectra.

When it is necessary to eliminate astigmatism and thereby make it possible to apply such methods, the concave grating is usually combined with a cylindrical lens or a spherical mirror. However, the addition of these auxiliary apparatus is done at the expense of the characteristic property of the concave grating, namely its self focusing property. Moreover the addition of such auxiliary instruments affects the intensity of light, especially in the range of the far ultraviolet, because the transmissibility and reflectivity of far ultraviolet light are very low. Thus it is rather difficult problem to obtain stigmatic spectral lines by means of a concave grating, and at the same time retain its superior characteristics.

If it were possible to device some improvement on the concave grating itself which should eliminate the astigmatism and yet retain its self focusing character, this should much enhance the usefulness of this form of grating. Along this line of thinking H. Harber[2] has proposed a theory of the Torus grating. His idea was based on the use of a toric surface instead of a concave spherical one, and with the ruling of usual equidistant parallel straight grooves on it. Then for a given angle of incident, there appear two points of non-astigmatism on the Rowland circle, and around these points astigmatism is naturally very small.

Harber's idea is a modification of the form of the grating surface, devised for the purpose of obtaining a non-astigmatic spectrum. In the present paper, another form of modification is presented, which features the usual spherical surface, but which introduces the idea of grooving in the form of a circular arc, the arcs being either of equal curvature or concentric. The center of sphere (i.e. center of groove O′ in Fig. 2) lies on the plane of the Rowland circle and on a line tangent to the grating surface, and the curvature is of a value comparable to the diameter of the Rowland circle. If the slit is situated on the point of intersection of the curvature sphere and the Rowland circles, stigmatic images are obtained at the same point and also at the opposit point against the grating O.

The theory of the grating was developed by H. G. Beutler[3], which we take as the starting point of the present discussion. As the grooves are of circular form, we transform the coordinates into suitable cylindrical coordinates (§ 3), and first search for the condition of non-astigmatism (§ 4). Then we examine how the line breadth is influenced by the modified form of the grooves (§ 5), and proceed

2) H. Harber: J.O.S.A. **40** (1950) 153.
3) H. G. Beutler: Ibid. **35** (1945) 311.

to discuss the coma of the grating (§ 6). Finally we mention the difference of the two groove-forms, namely that with concentric circles and that with circles of equal curvature (VII).

It may be a worthwhile to mention the present development of grating technique which makes possible the concentration of light intensity in a definite direction. This is obtained by giving a special form to the section of the grooves. As the stigmatic grating is intended for use in some definite direction, this technique of concentrating the intensity may be very useful in actual ruling practice.

2. Curved grating

The curved grating is defined as one which has equidistant curved grooves ruled upon a concave mirror. The forms of the curves for the grooves may be one of the following two: (1) lines all having equal curvature, as shown in Fig. 1 (a), and (2) lines all having the same concentric center, as in Fig. 1 (b). We will consider the second form first. This form can further be divided into two types. Suppose we fix O′ and move G freely, we obtain a set of concentric spherical surfaces which cut diffraction grooves on the grating surface. On the other hand, if we suppose the curved circles shown in Fig. 2 as projections of the grooves upon a plane, the real form of grooves is such as created by the intersection of a set of concentric cylinders and a spherical surface (the grating surface). For a theoretical consideration, the first type appears to be ideal.

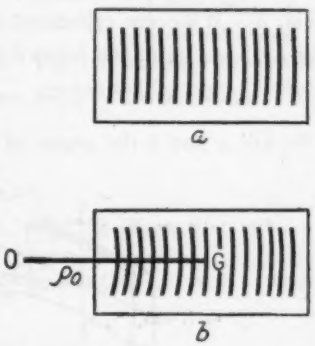

Fig. 1. Shape of the curved grooves, (a) equal curvature, (b) concentric circle.

Let the radius of the mirror be R and that of the curved line in the middle of the grating ρ_0 (see Fig. 2). The intersection of two spheres, one with its center at O′ and with radius ρ_0, and the other with center O and radius R, is a circle, which circle is none other than the curved groove itself. We can show from a simple geometrical consideration that the center of the groove circle, S, lies upon a Rowland circle. Therefore light which leaves S and is diffracted by the groove circle makes an image without aberration at the same point S. In the actual practice of ruling the grating, it would appear inconvenient to move the arm with the cutter around a fixed point O′ along a spherical envelope (case 1). The second case, namely, ruling along a cylindrical envelope should be more practical, and the

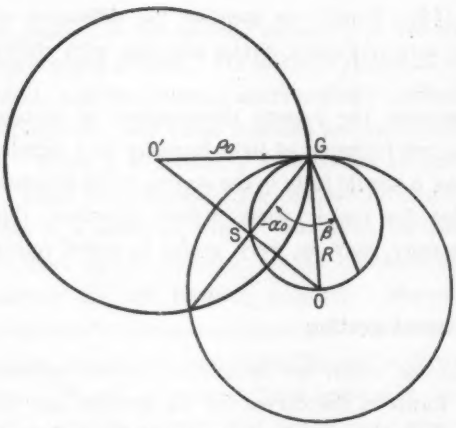

Fig. 2. Geometrical relation between the Rowland circle and the center of the curved groove.

difference between the spherical and cylindrical surfaces is small enough to be neglected, when the radius R and ρ_0 are sufficiently large compared to the size of the grating. In the following discussions we will treat the problem on the assumption that the grooves are on cylindrical surfaces.

3. Equation for the image formation

In the following, it is assumed that a ray leaving the point A (x_a, y_a, z_a) is reflected by the grating surface at the point P (x, w, l), and reaches the point B (x_b, y_b, z_b) (see Fig. 3). If we use cylindrical coordinates (r_a, α) and (r_b, β), they are related to (x_a, y_a) (x_b, y_b) in the following manner:

$$x_a=r_a\cos\alpha\,,\quad y_a=r_a\sin\alpha\,,\quad x_b=r_b\cos\beta\,,\quad y_b=r_b\sin\beta \qquad (1)$$

We call α and β the angles of incidence and diffraction respectively. If d is the

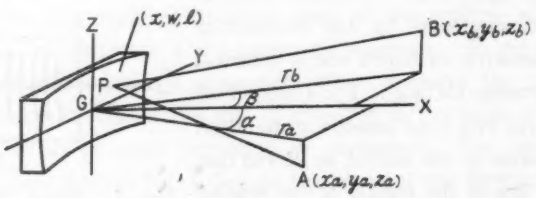

Fig. 3.

constant of the grating, the light path function used by Beutler[3] can be written as follow:

$$F=AP+BP+(w/d)m\lambda\,, \qquad (2)$$

where

$$AP=r_a-w\sin\alpha \qquad F_1$$

$$+\frac{1}{2}w^2\left(\frac{\cos^2\alpha}{r_a}-\frac{\cos\alpha}{R}\right)+\frac{1}{2}w^3\frac{\sin\alpha}{r_a}\left(\frac{\cos^2\alpha}{r_a}-\frac{\cos\alpha}{R}\right)$$

$$+w^4\frac{\sin^2\alpha}{r_a^2}\left(\frac{\cos^2\alpha}{r_a}-\frac{\cos\alpha}{R}\right)+\cdots. \qquad F_2$$

$$+\frac{1}{2}l^2\left(\frac{1}{r_a}-\frac{\cos\alpha}{R}\right)-\frac{l\cdot z_a}{r_a}+\frac{z_a^2}{2r_a} \qquad F_3$$

$$+\frac{1}{2}l^2 w\frac{\sin\alpha}{r_a}\left(\frac{1}{r_a}-\frac{\cos\alpha}{R}\right)+\frac{1}{2}w\frac{\sin\alpha}{r_a^2}(-2l\cdot z_a+z_a^2) \qquad F_4$$

$$+\frac{(w^2+l^2)^2}{8R}\left(\frac{1}{r_a}-\frac{\cos\alpha}{R}\right) \qquad F_5$$

$$+\frac{-w^4}{8r_a^2}\left(\frac{\cos^2\alpha}{r_a}-\frac{\cos\alpha}{R}\right)^2-\frac{3}{8}w^5\frac{\sin\alpha}{r_a^2}\left(\frac{\cos^2\alpha}{r_a}-\frac{\cos\alpha}{R}\right)^2 \qquad F_6$$

$$+\cdots\cdots$$

BP can be expressed by a similar formula, with the replacement $z_a\to z_b$, $\alpha\to\beta$, $r_a\to r_b$ and with F_1, $F_2\ldots$ replaced by F_1', F_2',..., m is the order of the spectrum and λ is the wave-length.

Since the grooves lie on cylindrical surfaces as mentioned above, it should be more convenient to use cylindrical coordinates $(x,\ \rho,\ \theta)$ having O′ as origin and θ as azimuthal angle (Fig. 4). The distance between O′ and the grating center G being ρ_0, we have

$$w=\rho\cos\theta-\rho_0\,,\qquad l=\rho\sin\theta \qquad (3)$$

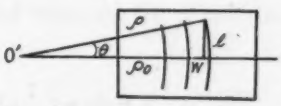

Fig. 4. Relation between the grating and the curved center.

For convenience we use W as the difference between ρ and ρ_0, namely,

$$W=\rho-\rho_0\,, \qquad (4)$$

then we have

$$w=(W+\rho_0)\cos\theta-\rho_0=W-(\rho_0+W)(1-\cos\theta)\,,\quad l=(\rho_0+W)\sin\theta \qquad (5)$$

As θ is small, we put $1-\cos\theta=\frac{\theta^2}{2}$, $\sin\theta=\theta-\frac{\theta^3}{6}$ in (5), then $(x,\ w,\ l)$ is transformed as follows:

$$(x,\ w,\ l)\to\{x,\ W-(\rho_0+W)(1-\cos\theta),\ (\rho_0+W)\sin\theta\}$$
$$\to\left\{x,\ W-(\rho_0+W)\frac{\theta^2}{2},\ (\rho_0+W)\left(\theta-\frac{\theta^3}{6}\right)\right\} \qquad (6)$$

If we put (6) into (2), we obtain

$$AP=r_a-\left\{W-(\rho_0+W)\frac{\theta^2}{2}\right\}\sin\alpha$$
$$+\frac{1}{2}\left\{W-(\rho_0+W)\frac{\theta^2}{2}\right\}^2\left(\frac{\cos^2\alpha}{r_a}-\frac{\cos\alpha}{R}\right)+\frac{1}{2}\cdots\cdots$$
$$+\frac{1}{2}(\rho_0+W)^2\left(\theta-\frac{\theta^3}{6}\right)^2\left(\frac{1}{r_a}-\frac{\cos\alpha}{R}\right)-\frac{(\rho_0+W)\left(\theta-\frac{\theta^3}{6}\right)}{r_a}z_a+\frac{z_a^2}{2r_a}$$

$$+\frac{1}{2}(\rho_0+W)^2\left(\theta-\frac{\theta^3}{6}\right)^2\left\{W-(\rho_0+W)\frac{\theta^2}{2}\right\}\frac{\sin\alpha}{r_a}\left(\frac{1}{r_a}-\frac{\cos\alpha}{R}\right)$$

$$+\left\{W-(\rho_0+W)\frac{\theta^2}{2}\right\}\frac{\sin\alpha}{2r_a}\left\{-2(\rho_0+W)\left(\theta-\frac{\theta^3}{6}\right)z_a+z_a^2\right\}$$

$$+\frac{1}{8R^2}\left[\left\{W-(\rho_0+W)\frac{\theta^2}{2}\right\}^2+(\rho_0+W)^2\left(\theta-\frac{\theta^3}{6}\right)^2\right]^2\left(\frac{1}{r_a}-\frac{\cos\alpha}{R}\right)$$

$$+\frac{-1}{8r_a^2}\left\{W-(\rho_0+W)\frac{\theta^2}{2}\right\}^4\left(\frac{\cos^2\alpha}{r_a}-\frac{\cos\alpha}{R}\right)^2$$

$$-\frac{3}{8r_a^2}\left\{W-(\rho_0+W)\frac{\theta^2}{2}\right\}^5\left(\frac{\cos^2\alpha}{r_a}-\frac{\cos\alpha}{R}\right)^2$$

$$+\cdots\cdots \tag{7}$$

Rearranging (7),

$$AP=r_a-W\sin\alpha \qquad C_1$$

$$+\frac{1}{2}W^2\left(\frac{\cos^2\alpha}{r_a}-\frac{\cos\alpha}{R}\right)+\frac{1}{2}W^3\frac{\sin\alpha}{r_a}\left(\frac{\cos^2\alpha}{r_a}-\frac{\cos\alpha}{R}\right)$$

$$+\frac{1}{2}W^4\frac{\sin^2\alpha}{r_a}\left(\frac{\cos^2\alpha}{r_a}-\frac{\cos\alpha}{R}\right)+\cdots \qquad C_2$$

$$+\frac{1}{2}\rho_0\theta^2\sin\alpha+\frac{1}{2}\rho_0^2\theta^2\left(\frac{1}{r_a}-\frac{\cos\alpha}{R}\right)-\frac{\rho_0\theta}{r_a}z_a+\frac{z_a^2}{2r_a} \qquad C_3$$

$$+\frac{1}{2}W\theta^2\sin\alpha-\frac{1}{2}\left(\frac{\cos^2\alpha}{r_a}-\frac{\cos\alpha}{R}\right)W\rho_0\theta^2+\left(\frac{1}{r_a}-\frac{\cos\alpha}{R}\right)W\rho_0\theta^2$$

$$+\frac{\sin\alpha}{2r_a}\left(\frac{1}{r_a}-\frac{\cos\alpha}{R}\right)W\rho_0^2\theta^2+\frac{\sin\alpha}{2r_a^2}\{-2\rho_0\theta z_a+z_a^2\}W-\frac{W\theta}{r_a}z_a \qquad C_4$$

$$+C_5+C_6+\cdots\cdots \tag{8}$$

For BP similarly,

$$BP=r_b-W\sin\beta \qquad C_1'$$

$$+\frac{1}{2}W^2\left(\frac{\cos^2\beta}{r_b}-\frac{\cos\beta}{R}\right)'+\frac{1}{2}W^3\frac{\sin\beta}{r_b}\left(\frac{\cos^2\beta}{r_b}-\frac{\cos\beta}{R}\right)$$

$$+\frac{1}{2}W^4\frac{\sin^2\beta}{r_b^2}\left(\frac{\cos^2\beta}{r_b}-\frac{\cos\beta}{R}\right)+\cdots \qquad C_2'$$

$$+\frac{1}{2}\rho_0\theta^2\sin\beta+\frac{1}{2}\rho_0^2\theta^2\left(\frac{1}{r_b}-\frac{\cos\beta}{R}\right)-\frac{\rho_0\theta}{r_b}z_b+\frac{z_b^2}{2r_b} \qquad C_3'$$

$$+\frac{1}{2}W\theta^2\sin\beta-\frac{1}{2}\left(\frac{\cos^2\beta}{r_b}-\frac{\cos\beta}{R}\right)W\rho_0\theta^2+\left(\frac{1}{r_b}-\frac{\cos\beta}{R}\right)W\rho_0\theta^2$$

$$+\frac{\sin\beta}{2r_b}\left(\frac{1}{r_b}-\frac{\cos\beta}{R}\right)W\rho_0^2\theta^2+\frac{\sin\beta}{2r_b^2}\{-2\rho_0\theta z_b+z_b^2\}W-\frac{W\theta}{r_b}z_b \qquad C_4'$$

$$+C_5'+C_6'+\cdots\cdots \tag{8}$$

In (8) the terms C_1, C_1', C_2 and C_2' are of the same form as F_1, F_1', F_2 and F_2' of the concave grating, therefore the general equation of the grating

$$\sin\alpha+\sin\beta=m\lambda/d \tag{9}$$

and the condition for the Rowland circle

$$r_a=R\cdot\cos\alpha\,,\qquad r_b=R\cdot\cos\beta \tag{10}$$

are valid for the curved grating as well.

4. Astigmatism

Next we proceed to the determination of the condition for the vertical focus. As Beutler pointed out, this condition is given by differentiating the term C_3+C_3' by $\rho_0\theta$, and equating it with zero:

$$\frac{\partial(C_3+C_3')}{\rho_0\partial\theta}=\left\{\sin\alpha+\left(\frac{1}{r_a}-\frac{\cos\alpha}{R}\right)\rho_0+\sin\beta+\left(\frac{1}{r_b}-\frac{\cos\beta}{R}\right)\rho_0\right\}\theta-\frac{z_a}{r_a}-\frac{z_b}{r_b}=0 \tag{11}$$

Since we are looking for a point to make the vertical focus, the law of reflection holds, and

$$\frac{z_a}{r_a}=\frac{-z_b}{r_b}. \tag{12}$$

Then (11) becomes

$$\sin\alpha+\left(\frac{1}{r_a}-\frac{\cos\alpha}{R}\right)\rho_0+\sin\beta+\left(\frac{1}{r_b}-\frac{\cos\beta}{R}\right)\rho_0=0 \tag{13}$$

Now let the angle between SG and the normal OG be $-\alpha_0$ and the distance of SG be r_{a0}, and we find that the relation

$$R\cos\alpha_0=\rho_0\sin\alpha_0=r_{a0} \tag{14}$$

holds. Substitute (14) into (13):

$$\sin\alpha+\left(\frac{1}{r_a}-\frac{\cos\alpha}{R}\right)\frac{\cos\alpha_0}{\sin\alpha_0}R+\sin\beta+\left(\frac{1}{r_b}-\frac{\cos\beta}{R}\right)\frac{\cos\alpha_0}{\sin\alpha_0}R=0 \tag{15}$$

This relation is satisfied by the following symmetrical conditions,

$$\sin\alpha+\left(\frac{1}{r_a}-\frac{\cos\alpha}{R}\right)\frac{\cos\alpha_0}{\sin\alpha_0}R=0\,,\quad \sin\beta+\left(\frac{1}{r_b}-\frac{\cos\beta}{R}\right)\frac{\cos\alpha_0}{\sin\alpha_0}R=0\,. \tag{16}$$

The first equation becomes

$$\frac{R}{r_a}\frac{\cos\alpha_0}{\sin\alpha_0}=-\sin\alpha+\frac{\cos\alpha\cdot\cos\alpha_0}{\sin\alpha_0}=\frac{\cos(\alpha_0+\alpha)}{\sin\alpha_0}\,,$$

hence

$$r_a=R\frac{\cos\alpha_0}{\cos(\alpha_0+\alpha)}=\frac{r_{a0}}{\cos(\alpha_0+\alpha)}\,. \tag{17}$$

Similarly we have

$$r_b=\frac{r_{a0}}{\cos(\alpha_0+\beta)}\,. \tag{18}$$

(17) and (18) represent one and the same straight line passing through S and O. Therefore a ray leaving any point along this line, after being diffracted by the grating, forms a vertical focus on the same line, and this is a secondary focal curve. If we let ρ_0 approach infinit, then r_{a0} approaches R and α_0 approaches O, and then the curved grating becomes concave one. Eq. (16) (17) become identical with eq. (39) of Beutler's paper.

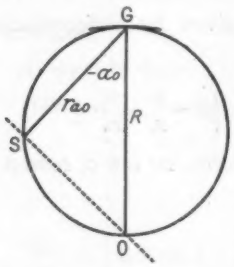

Fig. 5. Secondary focal line.

It is the outstanding characteristic of the curved grating that the secondary focal curve, i.e. the curve on which the image makes a vertical focus, intersects the Rowland circle. Therefore the light which enters the slit at S forms a stigmatic image either at S or at O. This fact can be explained in the following way. As it was stated in section II, the point S is the center of curvature of the groove, so the light leaving S reaches every point of the groove in the same phase and comes back to S again in the same phase; on the other hand, as the groove lies on a spherical surface, the light which leaves it at the same phase reaches O, the center of the curvature, in the same phase.

Let us next consider the case where the angle of incident α differs from $-\alpha_0$ (see Fig. 6). We will consider that the light emerges from the point M on the Rowland circle and forms the incident angle α. The problem is to look for the conditions for making a vertical focus.

We put

$$\alpha=-(\alpha_0+\Delta) \tag{19}$$

and introducing (14), (19) into (13) and noting the fact that M lies on the Rowland circle, (13) becomes

$$-\sin(\alpha_0+\Delta)+\left(\frac{1}{R\cos(\alpha_0+\Delta)}-\frac{\cos(\alpha_0+\Delta)}{R}\right)\frac{\cos\alpha_0}{\sin\alpha_0}R$$
$$+\sin\beta+\left(\frac{1}{r_b}-\frac{\cos\beta}{R}\right)\frac{\cos\alpha_0}{\sin\alpha_0}R=0\,,$$

and we accordingly obtain

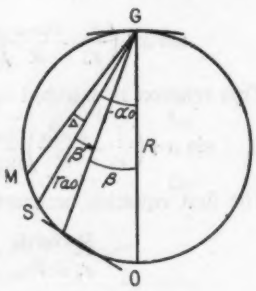

Fig. 6.

$$\frac{r_b}{R\cos\alpha_0}=\frac{1}{\cos(\alpha_0+\beta)-\tan(\alpha_0+\Delta)\sin\Delta} \tag{20}$$

(20) represents a hyperbola having its apex on the line GS. In Fig. 7 we show some examples, with $\alpha_0=60°$, $\Delta=2°$, 4°, 6°. We will again call these curves secondary focal curves. On the points where these secondary focal curves intersect with the Rowland circle, the images are stigmatic. The variation of β of this stigmatic point against the variation of Δ is shown in Fig. 8 (a), where β' is the angle of the stigmatic point measured from GS. The light which starts from S and forms a self-focusing images at S has a definite wave-length. The dotted line in Fig. 8 (a) shows the relation between the

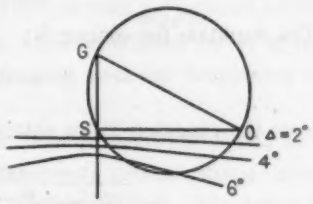

Fig. 7. Secondary focal curves.

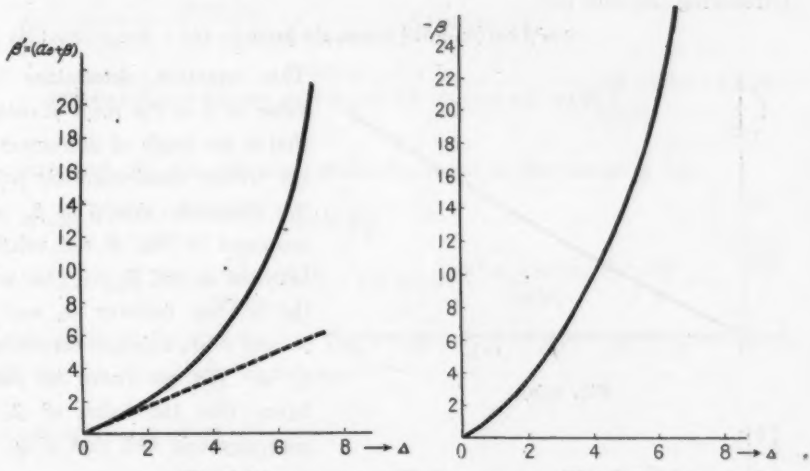

Fig. 8 (a) Fig. 8 (b)

Fig. 8. The point where astigmatism vanishes, that is intersection between the Rowland circle and the secondary focal curves, $\alpha_0=60°$.

incident and the emergent angles for this wave-length. If the two curves on Fig. 8 (a) coincide with each other, the stigmatic image is obtainable only for this definit wave-length. Fig. 8 (b) shows the variation of the stigmatic point from O.

If Δ in (19) varies, the relative position of the hyperbola to the Rowland circle also changes, and at a certain value of Δ they make contact with each other. In the vicinity of this point of contact, there will be formed a nearly stigmatic image. Let us seek for the condition of the contact. We will call s the difference of r_b and $R\cos\beta$, that is

$$s=r_b-R\cos\beta=\frac{R\cos\alpha_0}{\cos(\alpha_0+\beta)-\tan(\alpha_0+\Delta)\sin\Delta}-R\cos\beta \tag{21}$$

The condition for contact is:

$$1)\quad s=0 \qquad 2)\quad \frac{ds}{d\beta}=0$$

from the condition 1) we obtain

$$\frac{\cos\alpha_0}{\cos(\alpha_0+\beta)-\tan(\alpha_0+\Delta)\sin\Delta}=\cos\beta\,. \tag{22}$$

From the condition 2) we have

$$\frac{-\cos\alpha_0\{-\sin(\alpha_0+\beta)\}}{\{\cos(\alpha_0+\beta)-\tan(\alpha_0+\Delta)\sin\Delta\}^2}=-\sin\beta \tag{23}$$

Introducing (22) into (23),

$$\cos^2\beta\sin(\alpha_0+\beta)+\cos\alpha_0\sin\beta=0 \tag{24}$$

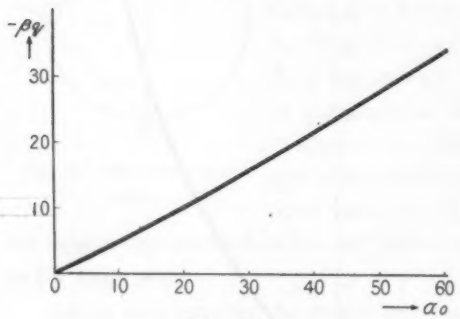

Fig. 9 (a)

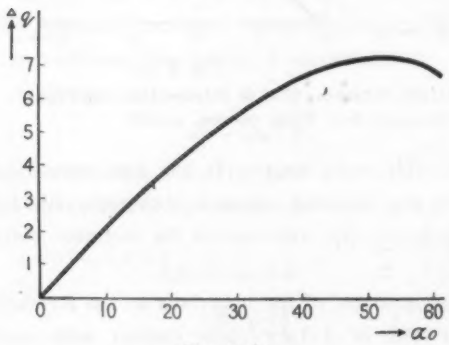

Fig. 9 (b)

Fig. 9. Relation between α_0 and $-\beta_q$ ($-\beta_q$ being the widest quasi-stigmatic point), and between α_4 and Δ for that point (Δ_q).

This equation determines the value of β at the point of cotact, that is the angle of diffraction at the widest quasi-stigmatic point. We designate this β as β_q, and represent in Fig. 9 the relation between α_0 and β_q, together with the relation between α_0 and Δ. β_q and Δ are uniquely determined by α. We see from the same figure that the value of β_q is approximately half that of α_0.

5. Broadening of spectral lines due to the curvature of the grooves

At the point where the condition of non-astigmatism is satisfied, it is not necessary to take into consideration the broadening of spectral lines due to the curvature of the grating grooves. However, when this condition does not strictly hold, we must

expect a broadening of the lines.

The condition of non-astigmatism was given by (11), namely $\frac{\partial}{\partial(\rho_0\theta)}(C_3+C_3')=0$. If this differential derivative does not vanish, the value multiplied by r_b gives the broadening of the focal point, and its y-component gives the broadening of spectral lines.

Suppose the amount of the broadening of the focal point corresponding to a point of a slit is expressed by l_s, then $l_s\theta/\cos\beta$ represents the broadening along the Rowland circle, which gives the broadening of spectral lines. We define β_0 as β at the stigmatic point, and we will examines how the broadening varies with $\delta\beta=\beta-\beta_0$.

From (21)

$$s=\frac{R\cos\alpha_0}{\cos(\alpha_0+\beta_0+\delta\beta)-\tan(\alpha_0+\Delta)\sin\Delta}-R\cos(\beta_0+\delta\beta)$$
$$=\frac{R\cos\alpha_0}{\cos(\alpha_0+\beta_0)\cos\delta\beta-\sin(\alpha_0+\beta_0)\sin\delta\beta-\tan(\alpha_0+\Delta)\sin\Delta}-R\cos(\beta_0+\delta\beta) \tag{25}$$

We introduce (21) into (25) and expand the result in the power of $\delta\beta$:

$$s=R\left(\frac{\cos(\alpha_0+\beta_0)\cos^2\beta_0}{\cos\alpha_0}+\sin\beta_0\right)\delta\beta$$
$$+R\left(\frac{\cos(\alpha_0+\beta_0)\cos^3\beta_0}{\cos\alpha_0}+\cos\beta_0+2\frac{\sin^2(\alpha_0+\beta_0)\cos^2\beta_0}{\cos^2\alpha_0}\right)\frac{\delta\beta^2}{2}+\cdots$$

If the length of the grooves is l, the broadening of the spectrum δp, is expressed with the use of $l_s=l\frac{s}{r_b}$ as follows;

$$\delta p=l_s\theta/\cos\beta=\frac{s}{r_b}l\theta\frac{1}{\cos\beta}$$
$$=l\theta\left\{\left(\frac{\sin(\alpha_0+\beta_0)}{2\cos\alpha_0}+\frac{\sin\beta^0}{\cos^2\beta_0}\right)\delta\beta+\left(\frac{\cos(\alpha_0+\beta_0)}{2\cos\alpha_0}+\frac{1}{2\cos\beta_0}+\frac{\sin^2(\alpha_0+\beta_0)}{\cos^2\alpha_0}\right.\right.$$
$$\left.\left.+2\frac{\sin(\alpha_0+\beta_0)}{\cos\alpha_0}\frac{\sin\beta}{\cos\beta_0}+2\frac{\sin^2\beta_0}{\cos^2\beta_0}\right)\delta\beta^2+\cdots\cdots\right\} \tag{26}$$

Table I

$\delta p=1\,\mu$							
$\beta_0=$	$-30°$	$-25°$	$-20°$	$-15°23'$	$-10°$	$-5°$	$-0°$
$\delta\beta-$	45′	1°1′	2°10′	5°1′	3°29′	1°36′	55′
$\delta\beta+$	48′	1°53′	10°33′	5°1′	1°59′	1°11′	51′
$\delta p=5\,\mu$							
$\beta_0=$	$-30°$	$-25°$	$-20°$	$-15°23'$	$-10°$	$-5°$	$-0°$
$\delta\beta-$	3°18′	5°24′	7°6′	11°15′	18°7′	24°35′	5°46′
$\delta\beta+$	5°12′	17°3′	15°29′	11°15′	7°9′	5°1′	3°50′

As an example we take $R=600$ cm., $2l=7$ cm., width$=15$ cm. and $\alpha_0=30°$, and obtain the relation between $\delta\beta$ and δp. From graphs representing this relation we choose $\delta p=1\,\mu$ and $5\,\mu$. The values are given in Table I, where $\delta\beta+$ and $\Delta\beta-$ are the angles between β_0 and the $+$ and $-$ directions respectively.

Similary the values for the grating for $R=600$ cm., $2l=7$ cm., width$=15$ cm. and $\alpha_0=60$ are as follows:

when $\beta_0=\beta_a$ $\quad\delta p=1\,\mu \quad \Delta\beta=2°11'$

$\quad\delta p=5\,\mu \quad \Delta\beta=5°1'$

Besides the broadening of lines above discussed, there is of course the width of the lines due to the diffraction itself. The diffraction width of the spectrum varies according to the wave-length as well as to the angle of incidence and diffraction, and for the usual 6 meter grating, its amount is about $15\,\mu\sim30\,\mu$. Therefore if we use the curved grating in such a range as would render the broadening due to the curvature of the grooves less than $5\,\mu$, the effect upon the resolving power should not be more than 10% (c.f. Beutler).

6. Coma

Up to now we have discussed the astigmatism and the effect of the curvature of the grooves. In addition, the spherical mirror causes coma, which is represented by C_4+C_4' in the light path function formula (8). The conditions for the elimination of this can be derived by differentiating the term C_4+C_4' with respect to $\rho_0\theta$ or W. Since astigmatism is equal to zero, we can put $z_b=0$ if $z_a=0$.

Then we obtain

$$\frac{\partial(C_4+C_4')}{\rho_0\partial\theta}=\left\{\sin\alpha-\left(\frac{\cos^2\alpha}{r_a}-\frac{\cos\alpha}{R}\right)\rho_0+2\left(\frac{1}{r_a}-\frac{\cos\alpha}{R}\right)\rho_0+\frac{\sin\alpha}{r_a}\left(\frac{1}{r_a}-\frac{\cos\alpha}{R}\right)\rho_0^2\right\}W\frac{\theta}{\rho_0}$$
$$+\left\{\sin\beta-\left(\frac{\cos^2\beta}{r_b}-\frac{\cos\beta}{R}\right)\rho_0+2\left(\frac{1}{r_b}-\frac{\cos\beta}{R}\right)\rho_0+\frac{\sin\beta}{r_b}\left(\frac{1}{r_b}-\frac{\cos\beta}{R}\right)\rho_0^2\right\}W\frac{\theta}{\rho_0} \tag{27}$$

$$\frac{\partial(C_4+C_4')}{\partial W}=\frac{1}{2}\left\{\sin\alpha-\left(\frac{\cos^2\alpha}{r_a}-\frac{\cos\alpha}{R}\right)\rho_0+2\left(\frac{1}{r_a}-\frac{\cos\alpha}{R}\right)\rho_0+\frac{\sin\alpha}{r_a}\left(\frac{1}{r_a}-\frac{\cos\alpha}{R}\right)\rho_0^2\right\}\theta^2$$
$$+\frac{1}{2}\left\{\sin\beta-\left(\frac{\cos^2\beta}{r_b}-\frac{\cos\beta}{R}\right)\rho_0+2\left(\frac{1}{r_b}-\frac{\cos\beta}{R}\right)\rho_0+\frac{\sin\beta}{r_b}\left(\frac{1}{r_b}-\frac{\cos\beta}{R}\right)\rho_0^2\right\}\theta^2 \tag{28}$$

The terms in parenthesis of (27) and (28) are of similar form, and we have

$$\{\ \}=\sin\alpha+\left(\frac{\cos^2\alpha}{r_a}-\frac{\cos\alpha}{R}\right)\rho_0+\left(\frac{1}{r_a}-\frac{\cos\alpha}{R}\right)\rho_0-\left(\frac{\cos^2\alpha}{r_a}-\frac{\cos\alpha}{R}\right)\rho_0$$
$$+\frac{\sin\alpha}{r_a}\left(\frac{1}{r_a}-\frac{\cos\alpha}{R}\right)\rho_0^2$$

$$=\sin\alpha+\left(\frac{1}{r_a}-\frac{\cos\alpha}{R}\right)\rho_0+\frac{\sin\alpha}{r_a}\rho_0\left\{\sin\alpha+\left(\frac{1}{r_a}-\frac{\cos\alpha}{R}\right)\rho_0\right\} \tag{29}$$

Then (28) becomes

$$\frac{\partial(C_4+C_4')}{\partial W}=\left[\sin\alpha+\left(\frac{1}{r_a}-\frac{\cos\alpha}{R}\right)\rho_0+\sin\beta+\left(\frac{1}{r_b}-\frac{\cos\beta}{R}\right)\rho_0\right.$$
$$\left.+\frac{\sin\alpha}{r_a}\rho_0\left\{\sin\alpha+\left(\frac{1}{r_a}-\frac{\cos\alpha}{R}\right)\rho_0\right\}+\frac{\sin\beta}{r_b}\rho_0\left\{\sin\beta+\left(\frac{1}{r_b}-\frac{\cos\beta}{R}\right)\rho_0\right\}\right]\theta^2 \tag{30}$$

If (30) assumes the value zero, the condition for elimination is satisfied. From (16), (30) becomes zero on the line OS. Therefore light which enters from S forms images at O and S free of coma. In the case of astigmatism, there was a secondary focal curve corresponding to an arbitrary point M and on that curve astigmatism was zero. However in the present case for coma, there does not exist such a condition for any position of M, and S and O are the only points which give images without coma. The amount of coma is largest at β_0, namely at the stigmatic point. In Fig. 10 we show the amount of coma at β_0 in microns against α_0 calculated for a grating of 6 meters, using the formula (30). As may be seen from it, this is less than 5 μ for $\alpha_0=30°$. This is just equal to the value obtained for astigmatism, so we can neglect the effect of coma upon the resolving power for gratings that have an angle of α_0 less than 30°.

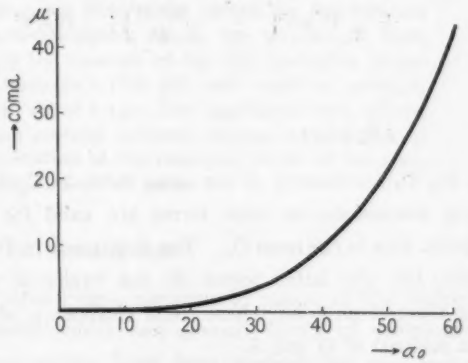

Fig. 10. Amount of coma at the β_0 point for 6 m. grating where secondary focal curve contacts Rowland circle.

7. The case of equal curvature grooves

We have hitherto discussed the characteristics of the grating with concentric curved grooves. As mentioned in the introduction, we can consider an alternative form, namely that having all the grooves of equal curvature (Fig. 1 (a)). In this case we can use the same cylindrical coordinate as before, and the formulae (1) and (2) may again be used. As the curvature of the grooves is a common value in this case, we must use instead of (3) or (5)

$$l=\rho_0\sin\theta=\rho_0\left(\theta-\frac{\theta^3}{6}\right)$$

$$\omega=W-\rho_0(1-\cos\theta)=W-\rho_0\frac{\theta^2}{2} \tag{31}$$

Here we use W as defined by (4). Introducing (31) into the Beutler's formula we obtain, instead of (8),

$$AP=r_a-W\sin\alpha \qquad D_1$$

$$+\frac{1}{2}W^2\left(\frac{\cos^2\alpha}{r_a}-\frac{\cos\alpha}{R}\right)+\frac{1}{2}W^2\frac{\sin\alpha}{r_a}(\qquad)+\cdots \qquad D_2$$

$$+\frac{1}{2}\rho_0\theta^2\sin\alpha+\frac{1}{2}\rho_0^2\theta^2\left(\frac{1}{r_a}-\frac{\cos\alpha}{R}\right)-\frac{\rho_0\theta^2}{r_a}z_a+\frac{z_a^2}{2r_a} \qquad D_3$$

$$+\frac{-1}{2}W\rho_0\theta^2\left(\frac{\cos^2\alpha}{r_a}-\frac{\cos\alpha}{R}\right)+\frac{1}{2}W\rho_0^2\theta^2\frac{\sin\alpha}{r_a}\left(\frac{1}{r_a}-\frac{\cos\alpha}{R}\right)$$

$$+\frac{W\sin\alpha}{2r_a}(-2\rho_0\theta z_a+z_a^2) \qquad D_4$$

$$+D_5+D_6+\cdots.$$

D_1, D_2, D_3 are exactly of the same form as C_1, C_2, C_3, and therefore the foregoing discussions on these terms are valid for the present case. A difference appears first in the term D_4. The first term in D_4 becomes zero on the Rowland circle, but the latter terms do not vanish at any position. Therefore in this case there is no point where coma disappears, although in the former case this was realized at O and S.

8. Conclusion

For curved grating, either with concentric circular grooves or with equidistant equal curvature grooves, we can conclude the following:

1) For a particular angle of incidence, the curved grating can eliminate astigmatism at two points on the Rowland circle.

2) If astigmatism is not zero, it causes a broadening of the spectral lines, neverthereless when astigmatism is small, thebr oadening of the spectral lines is also very small.

Concerning coma, the former type, namely with concentric circular grooves, has points where coma disappears, but the latter, with equal curvature grooves, has no such point.

The author expresses his hearty gratitude to Professor Fujioka for his deep interest and kind advice bestowed on the present work. The author is also much indebted to other members of the Institute for many valuable discussions.

Construction of a Grating Spectrometer

Takeshi NAMIOKA

Institute for Optical Research, Tokyo University of Education

(Received Dec. 15, 1953)

A 15,000 line per inch, 54-cm grating spectrometer based on the Seya mounting is described, which is designed to simplify the mechanism of wavelength change, to provide for automatic scanning, photoelectric and photographic measurements, and which lends itself to reconstruction for use as 1- or 3-meter gratings.

The entrance and exit slits are fixed; the grating rotates about a vertical axis through the center of the grating and different wavelengths are obtained in good focus over a wide range simply by this rotation of the grating. As the instrument now stands the wavelength limit on the long side, imposed by the response of the 1P21 multiplier phototube, is 6200 A but if for instance a PbS cell were used as detector, this limit should be rised to about 1.4 μ. The applicable area of the ruled surface of the grating remains constant during the rotation of the grating, and so no diminution of the resolving power of the spectrum occurs throughout the whole wide range.

1. Introduction

Recently the techniques of measuring a spectrum by means of the multiplier photo-tube have made great development and several forms of spectrometer suitable for photo-electric measurements have been devised for this purpose. These spectrometers are roughly devided into three main classes;

(1) prism spectrometers such as the Beckman type,

(2) plane grating spectrometers or concave grating spectrometers of the Wadsworth mounting type,

(3) concave grating spectrometers such as the Baird type.

In the first place, the Beckman spectrometer[1] is of a very compact design and its operation very easy, but measurement in the region below 1800 Å is impossible because of the use of a quartz prism in its dispersion system.

In the second place, the plane grating spectrometer[2], the Ebert mounting type[3] etc., and the Wadsworth mounting concave grating spectrometer[4] have

1) Kaye, Canon and Devaney: J.O.S.A., **41** (1951) 658;
Wilbur Kaye and R. G. Devaney: J.O.S.A., **42** (1952) 567.
2) T. B. Thomas and E. E. Schneider: J.O.S.A., **41** (1951) 1002.
3) William G. Fastie: J.O.S.A., **42** (1952) 641, 647.
4) G. P. Koch, W. J. Taylor and H. L. Johnston: J.O.S.A., **41** (1951) 125.

excellent characteristics, but as the reflectivity of their collimating mirrors is very small in the extreme ultraviolet region they cannot be used in this region unless the standard mirrors are replaced by one made of some material of superior reflectivity to be found.

In the case of the Baird type[5], which is the only vacuum spectrometer in the market at present, the concave grating is moved along the Rowland circle for change of wavelength, which causes the beam emerging from the exit slit to turn at the same time, so that the incident beam does not remain pointed at the center of the grating. This makes it difficult to make measurements over a wide range of wavelengths because of the diminution caused on its resolving power. A further, structural, disadvantage inherent in this type is the necessity of a considerably large vessel.

Thus, so far no spectrometer has yet been constructed which makes possible measurements to be made with a constant performance over the whole range of the spectrum. Recently, Seya[6] has reported on a new mounting for the concave grating suitable for use in a spectrometer, and he suggests in his paper the possibility of the construction of a spectrometer with a simplified mechanism based on his mounting.

The writer has constructed a grating spectrometer based on Seya's theory which will be briefly summarized in the following section.

2. Seya's Theory on Mounting of Concave Grating

Seya has calculated the conditions under which may be obtained an invariably sharp spectral image extending over a wide range where use is made of fixed entrance and exit slits and of a grating rotation about a vertical axis through its center.

Now, let α and β be the angles between the grating normal and the incident and diffracted rays, respectively. Further let r and r' be the distances from the grating center respectively to the entrance and exit slits. Then, the focal condition for the concave grating is expresed by

$$w\left(\frac{\cos^2\alpha}{r}-\frac{\cos\alpha}{R}+\frac{\cos^2\beta}{r'}-\frac{\cos\beta}{R}\right)$$
$$+\frac{3}{2}w^2\left[\frac{\sin\alpha}{r}\left(\frac{\cos^2\alpha}{r}-\frac{\cos\alpha}{R}\right)+\frac{\sin\beta}{r'}\left(\frac{\cos^2\beta}{r'}-\frac{\cos\beta}{R}\right)\right]+\cdots=0, \quad (1)$$

5) R. Tousey, F. S. Johnson, John Richardson and Nestor Toran: J.O.S.A. **41** (1951) 696,
Y. Fujioka and R. Ito: Science of Light, **1** (1951) 1.
6) M. Seya: Science of Light, **2** (1952) 8.

where R is the radius of curvature of the grating and w the width of the ruled portion.

Denoting the left-hand side of equation (1) by f and neglecting terms of higher order, we have

$$f=\frac{\cos^2\alpha}{r}+\frac{\cos^2(\alpha-C)}{r'}-\frac{\cos\alpha+\cos(\alpha-C)}{R}, \tag{2}$$

where $C=\alpha-\beta$. As the variation of α is small, we may put $\alpha=\alpha_0+\Delta\alpha$ and expand the equation (2) with respect to $\Delta\alpha$. Then, by neglecting the higher order terms, f is expressed as follows:

$$\begin{aligned} f=&\frac{\cos^2\alpha_0}{r}+\frac{\cos^2(\alpha_0-C)}{r'}-\frac{\cos\alpha_0+\cos(\alpha_0-C)}{R}\\ &+\left\{\frac{-\sin 2\alpha_0}{r}-\frac{\sin 2(\alpha_0-C)}{r'}+\frac{\sin\alpha_0+\sin(\alpha_0-C)}{R}\right\}\Delta\alpha\\ &-\left\{\frac{-2\cos 2\alpha_0}{r}-\frac{2\cos 2(\alpha_0-C)}{r'}+\frac{\cos\alpha_0+\cos(\alpha_0-C)}{R}\right\}\frac{\Delta\alpha^2}{2}. \end{aligned} \tag{3}$$

The condition for f to become zero regardless of the value of $\Delta\alpha$ is given by

$$\begin{vmatrix} \cos^2\alpha_0 & \cos^2(\alpha_0-C) & -[\cos\alpha_0+\cos(\alpha_0-C)] \\ -\sin 2\alpha_0 & -\sin 2(\alpha_0-C) & \sin\alpha+\sin(\alpha_0-C) \\ -2\cos 2\alpha_0 & -2\cos 2(\alpha_0-C) & \cos\alpha_0+\cos(\alpha_0-C) \end{vmatrix}=0. \tag{4}$$

Among the three solutions of the determinant (4), we adopt the solution which satisfies the condition, $\frac{\partial C}{\partial\alpha_0}=0$, because we wish to obtain a solution in which C, r and r' are always invariant and f always zero regardless of change of α around α_0. Such a solution is unique and has a maximum point at $C\fallingdotseq 70°$. But we have further to examine the conditions,

$$\left[\frac{\partial r}{\partial\alpha_0}\right]_{C=\text{const.}}=0,\quad \left[\frac{\partial r'}{\partial\alpha_0}\right]_{C=\text{const.}}=0 \quad\text{and}\quad \left[\frac{\partial r'}{\partial\alpha_0}\right]_{\substack{r=\text{const.}\\ C=\text{const.}}}=0.$$

From the result of further examination we have $C=70°15'$, $R/r=1.22247$. If we adopt the values cited above, the change of r' is smaller than 0.15 mm when we use a 1-meter concave grating within the range $\alpha=21°30'\sim35°7.5'$, corresponding to wavelength range of 6600~0 Å.

Therefore, by applying the results described above we are in a position to construct a spectrometer suitable for photoelectric measurements with a simplified mechanism.

3. Spectrometer

A spectrometer based on the Seya mounting has been constructed as follows: The measurable range extended approximately from 500 to 6200 Å, limited by the response of the 1P21 multiplier photo-tube. Spectral lines could be resolved down to 2 Å. In this spectrometer, a 15,000 line per inch, 54-cm concave grating with a ruling area of 25×30 mm was used and the values $C=70°15'$ and $r=44$-cm were adopted.

A schematic diagram of the spectrometer is shown in Fig. 1. The main vessel containing the grating and a part of the driving system is constructed from a seamless steel tube of 31.4-cm inside diameter and 33-cm length. At the one end of

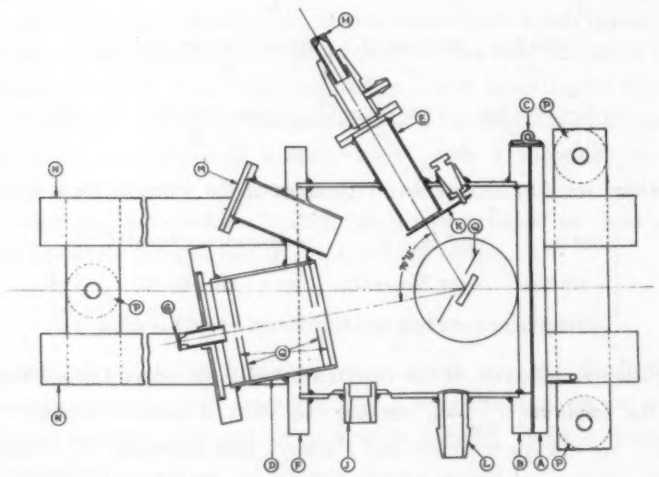

Fig. 1. Schematic diagram of the spectrometer.

the main vessel, a door A is attached to the flange B by a hinge C and these are kept air-tight by means of a rubber gasket placed in the groove on the flange surface and bolted. The branch tubes D, of 6 inch inside diameter, and E, of 2 inch inside diameter, are both made of seamless steel tubes and are welded respectively to the other end plate F and to one wall of the main vessel. The photographic plate holder or exit slit G is attached to the free end of D, while the entrance slit H is fixed onto the free end of E. Furthermore, by adding tubes of such diameter as to fit into the free ends of tubes D and E, it may be converted very easily into a long radius grating spectrometer of 1- to 3-meters. J, K and M are respectively an air-tight joint of the driving system, a shutter, and a

vacuum joint connected to the main exhaust line. L is a vacuum joint provided for the insertion of pressure gauges. The entire spectrometer is welded onto two parellel iron I-shaped beams N and its position may be adjusted by means of three jackscrews P.

The system of light baffles Q is designed to trap and to dissipate the zero order spectrum and spectra of other orders and wavelengths. They are set in front of the grating and also on the rings attached inside the branch tube D.

The grating holder and a part of the driving system are attached rigidly to the iron base plate in the main vessel. The grating can be independently rotated about either the x, y or z axes and translated along either the x or y axes. The driving system of the grating is shown schematically in Fig. 2. The arm A is

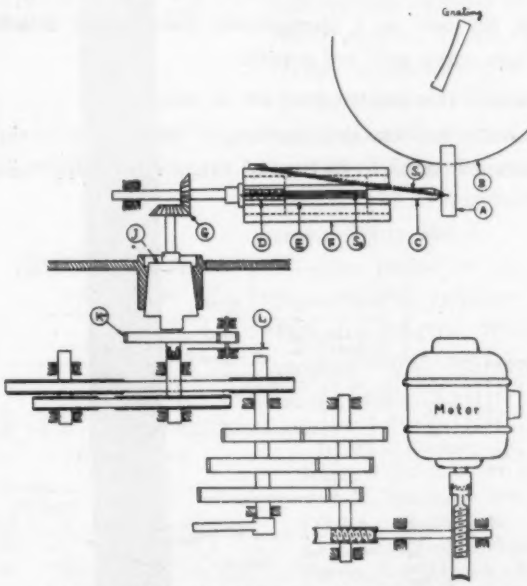

Fig. 2. Schematic diagram of the scanning system.

fastened to the disk B of the grating holder and pushes against the rounded end of the plunger C by the action of the spring S_1. The other end of the steel plunger C, of 6-mm diameter, rests against a sleeve E sliding along a tapered groove F. The position of E along the groove is set by a screw D, of 6-mm diameter, 35-mm length and with a pitch of 1-mm. C and D are aligned along a common center line. D is connected to the external driving system by the bevel gears G through the air-tight joint J. The external driving system consists of

two pairs of beltpulleys, a three step gear box, two pairs of worm gears and motor. The axle of J and the final axle of the external driving system are connected by a universal joint in order to protect J from impairment caused by misalignment of the axes. The gear box provides us with a choice of three scanning speeds of 50, 25 and 12.5 Å per minute. The wavelength can be read direcly from graduated plates attached to the gears K and L. The error caused by the repeated scanning is not larger than 2 Å. The graduated plates were calibrated by mercury lines in the visible region, and by the 1216 Å Lyman α line of the hydrogen atom, and the 1608 Å Lyman band of the hydrogen molecule in the extreme ultraviolet region.

The spectrometer can be converted into a photographic spectrograph by replacing the exit slit unit by a photographic plate holder attachment. Two exposures of 4.5-mm width each are possible.

The advantages of this spectrometer are as follows:

1) the mechanism for obtaining wavelength change is very simple,
2) the wavelength region to be covered extends from approximately 500 to 6200 Å,

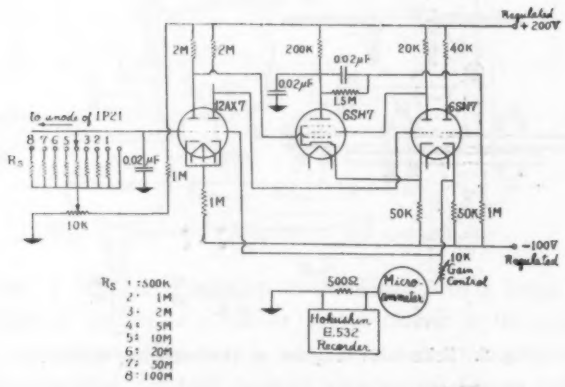

Fig. 3. Electrical circuit of the dc amplifier.

3) the whole area of the ruled surface of the grating can always be used and, therefore, no loss of resolving power is involved such as is caused in cases where the whole area is not always utilized,
4) the spectrometer may easily be converted into a photographic spectrograph,

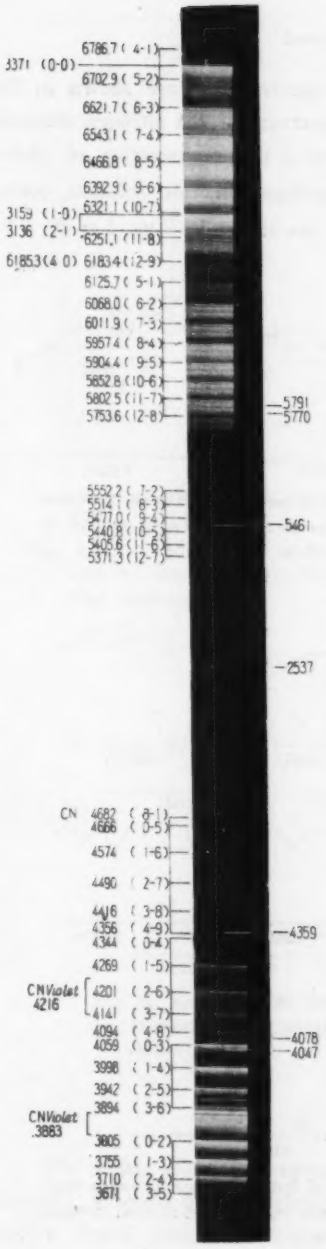

5) the spectrometer may easily be reconstructed into a long radius, 1- or 3-meter, grating spectrometer.

4. Detecting and Recording System

An RCA 1P21 multiplier photo-tube was used as a detector, contained in a light proof brass box. Additional stability is obtained by the use of an iron-resonance type voltage regulator on the AC 100 volt power supply. In the extreme ultraviolet region, measurement is made by means of fluorescence. Sodium salicylate[7] is used as a fluorescent material for its stability, its superior response and for the constancy of its quantum efficiency in the region 850 to 2400 Å.

The output of the 1P21 multiplier photo-tube is amplified and fed into a Hokushin Electric Works Model E. 532 recorder. The DC amplifier circuit[8] is shown in Fig. 3.

7) F. S. Johnson, K. Watanabe and R. Tousey: J.O.S.A., **41** (1951) 702,
K. Watanabe and Edward C. Y. Inn: J.O.S.A., **43** (1953) 32.

8) Keith Leon McDonald and Franklin S. Harris, Jr.: J.O.S.A., **42** (1952) 321, Valley and Wallman: *Vacuum Tube Amplifiers*, p. 480, (1948).

Fig. 4. An example of the reproduction of photographed plates; Emission spectrum in the first and second positive system of nitrogen molecule. Light source is an air-filled discharge tube.

5. Spectrum Obtained

Several spectra obtained by the use of this spectrometer are shown in the following figures. Fig. 4 shows the emission spectrum of the nitrogen molecule in the region from 3670 to 6800 Å as an example of the reproduction of photographed plates. The absorption spectra of neodium chloride solution, iodine vapour and the emission spectra of N_2, CO, H_2 are shown in Figs. 5 to 9.

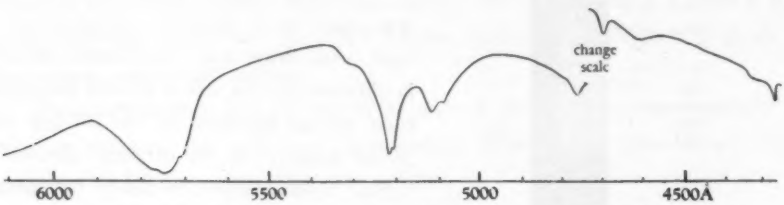

Fig. 5. Recording of the absorption spectrum of neodium chloride solution with 0.4-mm slit width. Scanning speed is 50 Å/min. Light source is an incandescent lamp.

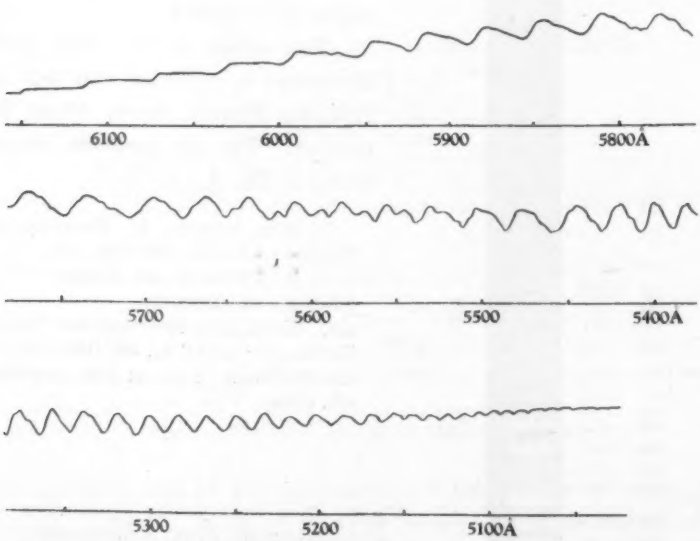

Fig. 6. Recording of the absorption spectrum of iodine vapour at room temperature. Slit width and scanning speed are 0.4-mm, 50 Å/min, respectively. Light source is an incandescent lamp.

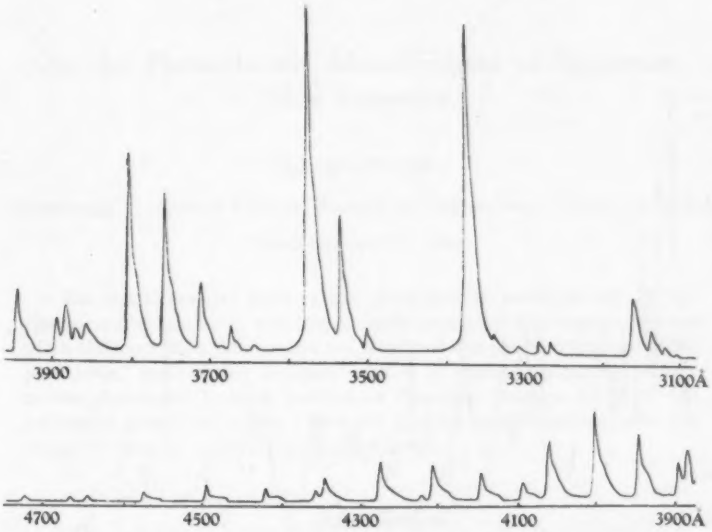

Fig. 7. Recording of the second positive emission bands of nitrogen molecule with 0.4-mm slit width, 50 Å/min scanning speed. Light source is an air-filled discharge tube.

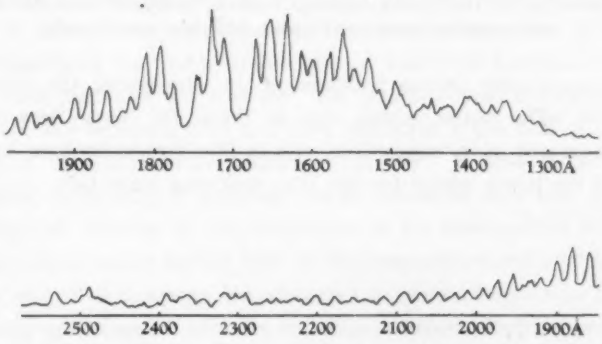

Fig. 8. Recording of the fourth positive emission bands of carbon monoxide. Slit width and scanning speed are 0.4-mm, 50 Å/min, respectively.

6. Acknowledgement

The writer wishes to express his heartfelt gratitude toward Professor Yoshio Fujioka, Director of the Institute, for his deep interest in the present work, and to Dr. Yoshio Tanaka for his kind gift of the RCA 1P21 multiplier photo-tube

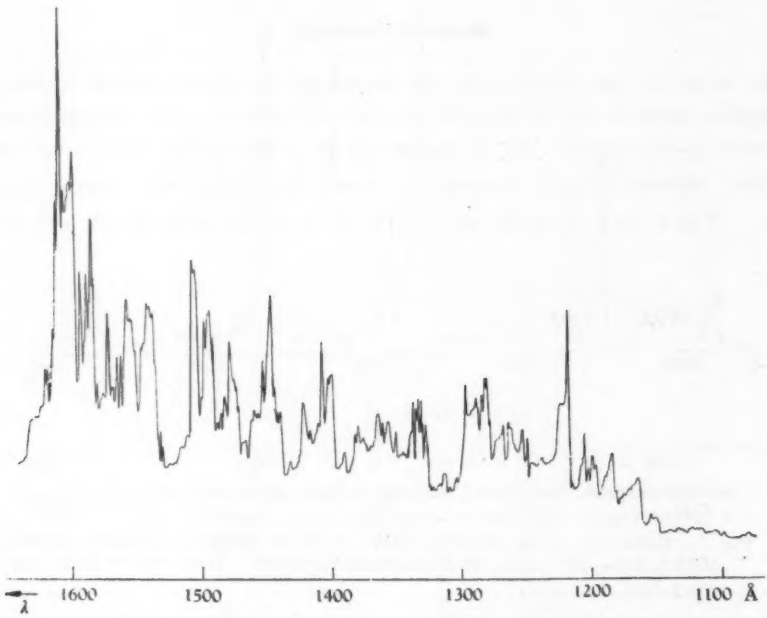

Fig. 9. Recording of the Lyman emission bands of hydrogen molecule. Slit width and scanning speed are 0.1-mm, 50 Å/min, respectively.

and for many valuable advices presented to him throughout the course of the present work. The writer wishes also to thank Dr. Masao Seya for his kind encouragement and many suggestions, and to Mr. Yoshimasa Sato for the construction of the power source for the 1P21 multiplier photo-tube.

On the Photoelectric Measurement of Spectrum Line Intensity

Shigeru FUJITA

Department of Applied Physics, Faculty of Engineering, Osaka University

(Received April 6, 1954)

The signal-to-noise ratio in the photoelectric measurement of the spectrum line intensity was theoretically calculated for the combination of an ordinary phototube and an a.c. amplifier and also for the multiplier phototube. Besides the ordinary method of applying constant voltage to the phototube, another method of applying voltage pulse to the multiplier phototube is also discussed, and the signal-to-noise ratio was found to increase appreciably in this case.

1. Introduction

Measurements of the wavelength of spectrum lines are now possible to be carried out with fairly high accuracy by the ordinary photographic method. But measurements of their intensity by the above method are not so satisfactory on the point of accuracy and speed because the intensity has to be calculated from the densitometry of the photographic plate on which the spectrum lines and also the calibration exposures are recorded. On the other hand the measurements of intensity are now becoming more and more important in the field of spectroscopy, especially in the spectroscopy applied to industry. In general, the accuracy of photographic photometry is relatively low as compared with that of the photoelectric method, because of the complexity of the photographic density and its dependency upon various factors such as the temperature and composition of the developer, etc. In comparison, the photoelectric method seems to be more accurate for intensity measurement since its response is linearly dependent on the incident energy on the photo-cathode. Nowadays, multiplier phototubes are easily available which have sufficient sensitivity in the region of ultra-violet and visible light, and are suitable for intensity measurements of weak radiation such as spectrum lines[1].

In this paper, the application of ordinary phototubes and also of multiplier phototubes to such measurements will be discussed theoretically.

1) R. W. Engstrom: J.O.S.A., **37** (1947) 420.

2. Theoretical Consideration

There are two kinds of the photo-emissive type of phototube, i.e. the ordinary phototube, and the multiplier phototube. The first kind has to be used ordinarily in conjunction with a proper amplifier with a high amplification factor, but the latter may be used without such elaborate accessories, since the latter is a combination of a photo-cathode and a high-gain secondary-emission multiplier and contained in a single envelope. However the former type is the only one suitable for the measurement of spectrum lines in the region of wavelengths longer than about 800 mμ where the multiplier phototubes have no sensitivity. For this reason the author intends to discuss first the ordinary phototube and amplifier combination, and then the multiplier phototube.

In the intensity measurement of a single spectrum line only a small quantity of energy is generally forthcoming, since, before the measurement, the single spectrum line must be separated from the others by some suitable device, such as the spectrometer, whereby only a very small portion of the total radiation energy from the light source will be allowed to enter through the entrance slit into the instrument, which then disperses it spatially into spectrum lines, only one of which is projected onto the photo-cathode through the exit slit. Consequently the photoelectric current thus generated is very weak and the ratio of the signal voltage to the noise voltage present in the phototube and the amplifier is an important factor in the measurement, especially on the point of accuracy.

In the following discussion, the sources of noise are assumed to be confined only to such as are theoretically unavoidable, since with proper precautions, other kinds of noise such as electro-static, electro-magnetic, microphonic, etc. could all be reduced to a negligible order of magnitude.

(*A*) *Photometry with a Combination of Ordinary Phototube and A.C. Amplifier*

In the following discussion the amplifier is assumed to be an a.c. amplifier, because this type is now considered to be preferable to the d.c. system. Although the radiation energy available for the measurement is generally smaller with the former than with the latter, the former is more stable and easier to construct when a high amplification factor is involved.

With the a.c. system of amplification, the light signal must be modulated to an alternating waveform by a suitable light chopper before being projected onto the photo-cathode. The intensity of the alternating light of square waveform can be expanded into a Fourier series as follows:

$$I=(2I_0/\pi)(\sin\omega t+1/3\cdot\sin 3\omega t+\ldots.), \qquad (1)$$

where I_0: the intensity of light signal before chopping,
I: the intensity projected onto the photo-cathode, and
$\omega=2\pi f$: the angular frequency of the light signal.

In a sharply-tuned amplifier for the photoelectric current, only the fundamental component of the series is effective in producing the output of the amplifier. Therefore, the root mean square (r.m.s.) value of the current is reduced to $\sqrt{2}/\pi$ of that corresponding to the initial intensity I_0, as seen from eq. (1). The sharply-tuned amplifier is ordinarily used to make the effect of the noise on the output as small as possible, but a synchronous rectifying system can also be adopted in the output circuit of the amplifier to reduce the noise, and in this case the amplifier need not be tuned so sharply as in the former case, and almost all the components of the series may appear in the output circuit without the involvement of further noise. Moreover the available input energy in this case, being just half of the initial intensity available to the d.c. system, is $\pi/2\sqrt{2}$ times that available in the case of a sharply-tuned a.c. amplifier.

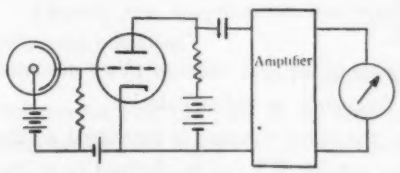

Fig. 1. Schematic diagram of the a.c. amplifier for the photoelectric current.

The ratio of the voltage generated by the photoelectric current to that by the noise is first calculated for the input circuit of the amplifier as shown in Fig. 1. Sources of the noise considered in the discussion are as follows:

1. Shot effect[2] in the signal photoelectric current and the dark current of the phototube.
2. Shot effect in the grid current of the first vacuum tube in the amplifier.
3. Thermal agitation of the charge in the resistor[3] used as the load resistor of the phototube.
4. Shot effect in the plate current of the first vacuum tube in the amplifier; this is the so-called tube noise and is expressed by the noise equivalent resistance in the input circuit.

The r.m.s. value of the total shot noise in the input circuit is given by the following equation:

$$\overline{E_s^2}=2e(i_g+i_a+i_S)R^2\int_{f_1}^{f_2}\frac{df}{(1+4\pi^2R^2C^2f^2)}, \qquad (2)$$

where i_S: the signal photoelectric current in the phototube,

2) W. Schottky: Ann. d. Physik, **57** (1918) 541.
3) H. Nyquist: Phys. Rev., **32** (1928) 110; J. B. Johnson: Phys. Rev., **32** (1928) 97.

i_d: the dark current in the phototube,
i_g: the grid current in the first vacuum tube,
R: the load resistance of the phototube,
C: the total dynamic capacity of the input circuit,
f: the frequency,
e: the electron charge, and
f_1 and f_2: the lower and the upper frequency limits of the passband of the amplifier.

The r.m.s. value of the thermal noise in the grid resistor, i.e. the load resistor of the phototube, is expressed by the following equation:

$$\overline{E_t^2}=4kTR\int_{f_1}^{f_2}df/(1+4\pi^2R^2C^2f^2)\,, \tag{3}$$

where T: the absolute temperature of the resistor, and
k: Boltzmann's constant.

The last one, i.e. the tube noise is given by the following equation:

$$\overline{E_{vt}^2}=4kTR_t\int_{f_1}^{f_2}df\,, \tag{4}$$

where R_t: the noise equivalent resistance of the first vacuum tube; assumed to be independent of the frequency in the calculation.

Since the mean square of the sum of the noise voltages is expressed as the sum of their mean squares, the total noise voltage $\overline{E_n^2}$ can be derived from the eqs. (2), (3) and (4) as follows:

$$\begin{aligned}\overline{E_n^2}&=\overline{E_s^2}+\overline{E_t^2}+\overline{E_{vt}^2}\\&=4kT[(1/2\pi C\tan^{-1}\{2\pi RC(f_2-f_1)/(1+4\pi^2R^2C^2f_1f_2)\}\cdot\{1+(2e/4kT)i_tR\}\\&\qquad+R_t(f_2-f_1)]\end{aligned} \tag{5}$$

where $i_t=i_g+i_d+i_S$.

On the other hand, the signal voltage E_S, generated by the signal photoelectric current through the resistance R, is given by the following equation:

$$E_S^2=i_S^2R^2/(1+4\pi^2R^2C^2f_0^2)\,, \tag{6}$$

where f_0: the signal frequency of the photoelectric current, and
i_S: for a sharply-tuned amplifier $i_S\propto\sqrt{2}\,I_0/\pi$, and for a wide-band amplifier $i_S\propto I_0/2$.

If the band width of the amplifier is sufficiently narrow and therefore the difference Δf between the upper and the lower frequency limits is also small enough as compared with the signal frequency f_0, the signal-to-noise ratio can approximately be expressed by the following equation:

$$E_S^2/\overline{E_n^2}=i_S^2R/4kT\Delta f\{1+R[(2e/4kT)i_t+4\pi^2C^2f_0^2R_t]\}\ . \qquad (7)$$

If the sensitivity of the phototube is denoted by S (amp./watt), and the incident light energy by L (watt)—which indicates the intitial value before chopping, eq. (7) is modified for the sharply-tuned amplifier as follows:

$$E_S^2/\overline{E_n^2}=(2L^2S^2/\pi^2)R/4kT\Delta f\{1+R[(2e/4kT)i_t+4\pi^2C^2f_0^2R_t]\} \qquad (8)$$

The case of the broad-band amplifier with a synchronous rectifier in the output circuit will not be discussed, because only the first constant factor on the right side of eq. (8) is different from that of the case of the sharply-tuned amplifier.

Judging from the above equation for the signal-to-noise ratio, it may be concluded that the following conditions must be satisfied in order to make the ratio as high as possible:

First, the following factors must be made as small as possible: the dark current of the phototube, the grid current and also the noise equivalent resistance of the first vacuum tube, the effective input capacity of the circuit, the light chopping frequency and the band-width of the amplifier.

Second, the coupling resistance must be made large enough to satisfy the following condition:

$$R\gg 1/\{(2e/4kT)i_t+4\pi^2C^2f_0^2R_t\}\ .$$

This means that the sum of the tube noises (which is expressed by the equivalent resistance in the input circuit) and the input voltage due to shot noise, which is linearly proportional to the value of the resistance (R), must to be made sufficiently greater than that due to the thermal noise of the resistor, which is proportional to the square root of the value of the resistance.

The band-width of the amplifier can not arbitrarily be made as small as possible, as will be deduced from the above equation, because the time of measurement or the respose time of the system is not independent of the band-width. The narrower the band-width, the longer the time of measurement. The load resistance of the phototube cannot be made greater than the dynamic differential grid resistance of the vacuum tube itself, because the former is necessarily shunted by the latter. The smaller the grid current, the greater the dynamic differential resistance. However, in general, the smaller the grid current, the smaller the plate current and therefore the greater the noise equivalent resistance. But fortunately by selecting a proper vacuum tube for the first tube, the noise equivalent resistance can be made negligibly small as compared with the load resistance of the phototube in the present case.

From the above equation, a low chopping frequency appears to be preferable, but the noise equivalent resistance of the vacuum tube increases in inverse pro-

portion to the frequency in the lower frequency range (so-called flicker noise[4]). Therefore an optimum frequency must be selected by taking both the flicker noise and the eq. (8) into consideration.

The minimum detectable power (min. det. power) was calculated for the first vacuum tube UY 38 with the eq. (8), assuming characteristics of the UY 38 to be:

grid current:	2.5×10^{-13} amp.,
input grid resistance:	10^{12} ohms,
noise equivalent resistance:	3.8×14^{4} ohms, and
total input capacitance:	30×10^{-12} farads.

The min. det. power is generally defined as the power of the signal which causes the same deflection in the output meter as that caused by the r.m.s. noise voltage. The light signal is assumed to be chopped at the frequency of 120 c.p.s., and the amplifier tuned to the same frequency with a band-width of 1 c.p.s. The phototubes are assumed to have the following sensitivity:

Sb-Cs phototube: 4.2×10^{-8} amp./microwatt or 0.13 electron/light quantum at the wavelength of 4000 A.

Cs phototube: 2.0×10^{-9} amp./microwatt or 0.0031 electron/light quantum at the wavelength of 8000 A.

The min. det. power for each phototube is as follows:

Sb-Cs phototube: 4.3×10^{-7} erg (or 8.7×10^{4} photons)/sec. at 4000 A,

Cs phototube: 9.0×10^{-8} erg (or 3.6×10^{8} photons)/sec. at 8000 A.

If a longer time than in the above case could be tolerated in measurements, some other suitable device could always be attached to the circuit of the amplifier in order to reduce the noise voltages. For example, the output of the a.c. amplifier can first be rectified and then the residual ripple voltages can be filtered off with an appropriate RC network, the resulting d.c. voltage being then read through a suitable d.c. amplifier. The steady component of the output in the case of no signal light on the photo-cathode can be eliminated by a substraction method and only the fluctuation will remain. Therefore the noise can be reduced down to a smaller value than previously. In this case, the longer the time constant of the network, the smaller the percentage of the noise (fluctuation) in the total output, i.e. the fluctuation decreases in inverse proportion to the square root of the time constant. For the time of measurement of one minute, the min. det. power will be reduced to the following values:

Sb-Cs phototube: 3.9×10^{-8} erg/min. (7.9×10^{3} photons/min.) at 4000 A.

4) J. B. Thompson et al: RCA Rev., **4** (1940) 269.

Cs-phototube: 8.2×10^{-7} erg/min. (2.0×10^{5} photons/min.) at 8000 A.

(*B*) *Photometry with the Multiplier Phototube*

Noise in the input circuit of the amplifier for the ordinary phototube is of great importance in the measurement of weak radiation, but it is generally far less than that in the case of the multiplier phototube. Since in the latter the current from the photo-cathode can generally be amplified up to a few million times in the secondary multiplication stages of the tube itself, the shot noise of the dark current produced in the photo-cathode would also be amplified to the same extent, and so the sole predominant noise in case of the multiplier may be assumed to be the shot noise of the output current of the multiplier itself, and the noise due to the conventional amplifier stage could all be neglected almost completely.

The noise in the output current of the multiplier consists of the following two factors: 1) the amplified shot noise in the dark and the signal photoelectric currents from the photo-cathode, and 2) the noise due to the fluctuation of the secondary multiplication process at each dynode stage. These are given by the following equation:[1]

$$\overline{I_n^2}=M^2\{1+1/(m-1)\}2e(i_d+i_S)\Delta f\,, \tag{9}$$

where I_n: the r.m.s. noise current at the anode of the multiplier,
M: the total amplification factor of the tube,
m: the multiplication factor of each dynode, and
i_d and i_S: the dark and signal photoelectric current at the cathode.

On the other hand, the signal photoelectric current at the anode is given by:

$$\overline{I_S^2}=M^2i_S^2\,. \tag{10}$$

From eqs. (9) and (10), the signal-to-noise ratio may be expressed by:

$$I_S^2/\overline{I_n^2}=i_S^2/\{(1+B)2e(i_d+i_S)\Delta f\}\,, \tag{11}$$

where $B=1/(m-1)$.

The min. det. power is calculated by eq. (11) for the multiplier phototube with the following characteristics:

dark current at the cathode: 5×10^{-14} amp.,
total amplification factor: 2×10^{6}, and
sensitivity at the anode: 7.4×10^{4} amp./watt at the wavelength of 4000 A.

The min. det. power is as follows:

7.9×10^{3} photons for $\Delta f=1$ c.p.s., and

720 photons for the measuring time of one min. at 4000 A.

The characteristics of a good multiplier phototube are, besides its high sensitivity, the frequency characteristics of the secondary multiplication stages. Signals from d.c. to more than 100 megacycles/sec. should be amplifiable in such multipliers. The higher frequency limit depends ordinarily not on the multiplier stage itself but rather on the following stage of the conventional amplifier as referred to in the ordinary case.

Therefore the multiplier can be used for the measurement of light signals of short duration with an accuracy higher than that of the combination of phototube and a.c. amplifier. When the latter is used to measure the light pulse, the band-width of the combination must be sufficiently wide in order to be capable of dealing with such kinds of signal, and therefore the load resistance of the phototube must also be reduced to a small value, which is determined by the dynamic capacity and the required frequency characteristics of the system. As mentioned above, the smaller the load resistance, the smaller the value of (S/N). This means that the time-change of a weak spectrum line of short duration can only be measured with the multiplier phototube, in which the ratio (S/N) is determined only by the tube itself and is therefore independent of the value of the load resistance.

To compare the sensitivity of the multiplier phototube with that of the combination of phototube and amplifier, the ratio of the signal-to-noise ratios in both cases was derived from eqs. (7) and (11) as follows:

$$\mathfrak{R}=\frac{(S/N)^2_{PM}}{(S/N)^2_{PT}}=\{1/(1+B)\}[1+i_g/(i_a+i_S)+(4kT/2e)\{1/(i_a+i_S)\}\{1/R+4\pi^2C^2f_0^2R_t\}]\,. \tag{12}$$

At room temperature ($T=300°\mathrm{K}$) this equation becomes:

$$\mathfrak{R}=\{1/(1+B)\}[1+i_g/(i_a+i_S)+(1/20)\{1/(i_a+i_S)\}\{1/R+4\pi^2C^2f_0^2R_t\}]\,. \tag{13}$$

From the above equation it is concluded that if

$$B<i_g/(i_a+i_S)+(1/20)\{1/(i_a+i_S)\{1/R+4\pi^2C^2f_0^2R_t\}$$

or $B<i_g/i_a+(1/20i_a)\{1/R+4\pi^2C^2f_0^2R_t\}$ for very weak incident light, (and this condition is almost always satisfied), the multiplier phototube has better S/N than the combination of phototube and amplifier.

The ratio $\mathfrak{R}$, which indicates the superiority of the multiplier, was calculated for various values of the parameters in the above equation, and the results are shown in the following table:

For a dark current smaller than 10^{-14} amp., the sensitivity of the multiplier phototube is 5 times greater than that of the phototube with the same photo-

Table 1. The ratio of $(S/N)^2$ of the multiplier phototube to that of the combination of phototube and amplifier.

Dark current (amp.)	Grid current (amp.)	$(S/N)^2_{PM}/(S/N)^2_{PT}$			
		Load resistance of the phototube			
		10^{11}	10^{12}	10^{13}	10^{14}
10^{-12}	10^{-12}	1.98	1.63	1.60	1.60
	10^{-13}	1.28	0.93	0.90	0.83
	10^{-14}	1.21	0.86	0.83	0.82
	10^{-15}	1.21	0.86	0.83	0.82
10^{-13}	10^{-12}	10.3	9.3	9.0	8.9
	10^{-13}	5.8	2.34	1.98	1.95
	10^{-14}	5.1	1.63	1.28	1.25
	10^{-15}	5.1	1.56	1.21	1.17
10^{-14}	10^{-12}	121	86	83	82
	10^{-13}	51	16.3	12.8	12.5
	10^{-14}	44	9.3	5.9	5.5
	10^{-15}	44	8.6	5.2	4.7
10^{-15}	10^{-12}	1.21	0.86	0.83	0.82×10^{3}
	10^{-13}	5.1	1.56	1.21	1.17×10^{2}
	10^{-14}	4.3	0.86	0.51	0.48×10^{2}
	10^{-15}	4.3	0.81	0.44	0.41×10^{2}

cathode, assuming that the dark current is the same in both case and the signal current is very low as compared with the dark.

For the measurement of a periodically-pulsed light signal, such as that from a condensed spark excited by an alternating current of a high voltage transformer, the following method will be advantageous in increasing the ratio S/N and therefore in measuring with higher sensitivity and accuracy.

In general the phototube need not have any sensitivity during the interval of time when no signal light is projected onto the photo-cathode, a high sensitivity being required only during the interval when the light is being projected. The sensitivity of the multiplier depends upon the voltage applied to the electrodes, and therefore if the voltage is reduced to a small value during the "dark" interval, then the dark current will be reduced along with the sensitivity to a negligible value, and the main part of the noise will not appear in the anode circuit during the unnecessary interval.

Judging from recent developments in the technique of electronic switches, such as those widely used in the circuit of Geiger-Mueller counters, electronic digital computors, etc., a method for applying the voltage to the multiplier

phototube only during predetermined "light" intervals should not be so difficult to devise.

In the discussion of the signal-to-noise ratio for the above case, the author assumed that the periodical light signal has a simple form as shown in Fig. 2, i.e. it was a sharp square wave of short duration (t sec.) and the period of one cycle was fairly longer (T sec.).

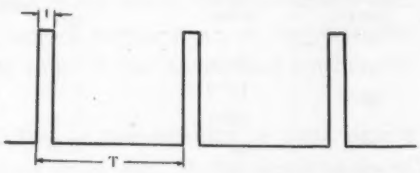

Fig. 2. Wave form of the periodically pulsating light.

First, for purposes of comparison, the ratio was calculated for the case of a constant voltage on the multiplier. Assume the number of photoelectrons generated by the signal light to be n_s per unit time and that of electrons due to the dark current n_d, then the number of photoelectrons during one cycle is $n_s t$ and that of dark electrons $n_d T$. (Hereafter the electrons due to the dark current will be termed "dark electrons.") If the time of measurement is τ, the number of the electrons is $(n_s t+n_d T)(\tau/T)$ during the measurement. Since the fluctuation in the number of electrons emitted by a source is equal to the square root of the total number, the fluctuation in this case is given by the following equation:

$$\begin{pmatrix}\text{fluctuation in the number}\\ \text{of total electrons}\end{pmatrix}_{V=\text{const}}=\begin{pmatrix}\text{the number of}\\ \text{total electrons}\end{pmatrix}^{\frac{1}{2}}=\{(n_s t+n_d T)(\tau/T)\}^{\frac{1}{2}}\ . \quad (14)$$

The number of signal photoelectrons on the other hand is equal to $n_s t(\tau/T)$. Therefore the ratio of the fluctuation in the number of total electrons to the number of signal photoelectrons is given by the following equation:

$$(\text{r.m.s. error})_{V=\text{const}}=(N/S)_{V=\text{const}}=(n_s t+n_d T)^{\frac{1}{2}}\Big/\left\{(n_s t)\cdot(\tau/T)^{\frac{1}{2}}\right\}\ . \quad (15)$$

The signal-to-noise ratio was calculated for the above mentioned case of the voltage pulse, assuming that all conditions excepting the voltage were the same as in the previous case. In this case, the number of the dark electrons during one cycle is reduced to $n_d t$, while that of the signal electrons remains the same as in the previous case, i.e. equal to $n_s t$. The number of total electrons is therefore $(n_s t+n_d t)(\tau/T)$, and the fluctuation in the number given by:

$$\begin{pmatrix}\text{fluctuation in the number}\\ \text{of total electrons}\end{pmatrix}_{V=\text{pulse}}=\{(n_s+n_d)(t\tau/T)\}^{\frac{1}{2}}\ . \quad (16)$$

The ratio of the fluctuation in the number of total electrons to the number of signal photoelectrons is given by the following equation:

$$(\text{r.m.s. error})_{V=\text{pulse}} = (N/S)_{V=\text{pulse}} = (n_s+n_d)^{\frac{1}{2}} \Big/ n_s(t\tau/T)^{\frac{1}{2}} . \qquad (17)$$

From the above two equations (15) and (17), the extent to which the r.m.s. error of measurement is reduced with the voltage pulse method, is derived as follows:

$$\mathfrak{R}' = (N/S)_{V=\text{const}} \Big/ (N/S)_{V=\text{pulse}} = \{(1+\alpha\beta)/(1+\beta)\}^{\frac{1}{2}} , \qquad (18)$$

where $\alpha = T/t$ and $\beta = n_d/n_s$.

In this equation α is always greater than unity, and so also $\mathfrak{R}'$, i.e. the method of voltage pulse always makes the accuracy of measurement higher than that with constant voltage. No restriction to the means of suppressing the sensitivity of the multiplier phototube during the dark period accrues from the above discussion, and any method could be adopted equally well.

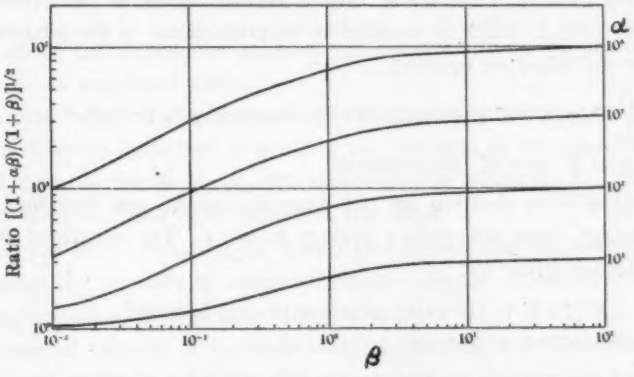

Fig. 3. Relation between $\mathfrak{R}'$ and β. $\mathfrak{R}'$: the ratio of the ratios $(S/N)_{V=\text{pulse}}$ and $(S/N)_{V=\text{const}}$; α: the ratio of the period of one cycle T to the duration of the light pulse t; β: the ratio of the number of dark electrons to that of signal photoelectrons.

The family of the curves in Fig. 3 shows the relation between $\mathfrak{R}'$ and α and β of eq. (16), β taken for the abscissa being the ratio of the number of the dark electrons to that of the signal electrons per unit time, and the ratio $\mathfrak{R}'$ taken for the ordinate. If T, the period of one cycle, is 1/100 sec., t, the duration of the pulse, is 10 microsec., and the ratio β is unity, then the ratio $\mathfrak{R}'$ is about 20, which means that; as compared with the constant voltage method, the accuracy of measurement with voltage pulse will be 20 times higher, or conversely, the time required for measurement with the same accuracy will be reduced by 1/400.

Of course, it must be remembered that in these discussions only the integrated intensity of the light is assumed to be measured and not the instantaneous values, and therefore some integrating device must be incorporated in the measuring circuit.

In the above discussion, the light pulse was assumed to be of the form of a square wave in order to simplify the calculation, but the ordinary light pulse, e.g. that from a condensed-spark, deviates in form from such an idealized assumption. It should resemble more a waveform such as expressed by the following equation:

$$I(t)=K\{\exp(-t/\tau_1)-\exp(-t/\tau_2)\},$$

where the constant τ_1, is assumed to be far greater than the constant τ_2, and $I(t)$ the instantaneous intensity of the light, t the time, and K a constant.

Calculations will first be carried out for this light pulse in the case of the voltage pulse method, as follows. The integrated number of the photoelectrons from time 0 to t, which is assumed to be proportional to the intensity, is expressed by the following equation:

$$\int_0^t K' I(t)dt=K'[\tau_1\{1-\exp(-t/\tau_1)\}-\tau_2\{1-\exp(-t/\tau_2)\}], \tag{19}$$

where K' and K'' are constants.

The number of dark electrons per unit time is constant, and therefore its integrated number from time 0 to t is given by $K'''t$. The integrated number of total electrons is given by:

$$K'''t+K''[\tau_1\{1-\exp(-t/\tau_1)\}-\tau_2\{1-\exp(-t/\tau_2)\}], \tag{20}$$

where K''' is a constant.

The fluctuation in the integrated number of total electrons is given by:

$$\left\{K'''t+K''[\tau_1\{1-\exp(-t/\tau_1)\}-\tau_2\{1-\exp(-t/\tau_2)\}]\right\}^{\frac{1}{2}}. \tag{21}$$

The ratio of the fluctuation in the total number to the number of signal photoelectrons is expressed as follows:

$$\left(\frac{N}{S}\right)_{V=\text{pulse}}=\frac{\left\{K'''t+K''[\tau_1\{1-\exp(-t/\tau_1)\}-\tau_2\{1-\exp(-t/\tau_2)\}]\right\}^{\frac{1}{2}}}{K''[\tau_1\{1-\exp(-t/\tau_1)\}-\tau_2\{1-\exp(-t/\tau_2)\}]}. \tag{22}$$

The ratio $\left(\frac{N}{S}\right)_{V=\text{pulse}}$ will be minimum at the moment when $d(N/S)/dt=0$. We can easily control the time t of the integration during which the sensitivity of the multiplier is not null, so that it is possible to satisfy the above condition, and therefore we are in a position to make the measurement during the most optimum

interval, thereby obtaining the highest accuracy.

According to the results of this calculation, it is concluded that the ratio $(N/S)_{V=\text{pulse}}$ is minimum at the moment when the value of t/τ_1 reaches 0.96–1.25 for the value of K''/K'''* between 0.50–0, respectively.

On the other hand, in case of constant voltage on the electrode, the number of photoelectrons will be $K''(\tau_1-\tau_2)$, and that of the dark electrons $K'''T$. Therefore the ratio (N/S) in this case is given as follows:

$$(N/S)_{V=\text{const}}=[K'''T+K''(\tau_1-\tau_2)]^{\frac{1}{2}}\Big/[K''(\tau_1-\tau_2)]\,. \tag{23}$$

From eqs. (22) and (23), the ratio of the ratio $(N/S)_{V=\text{pulse}}$ to $(N/S)_{V=\text{const}}$ may be derived as follows:

$$(N/S)_{V=\text{const}}\Big/(N/S)_{V=\text{pulse}}=\{e/(e-1)\}\cdot\left\{(1+\alpha'\beta')/\{\beta'+e/(e-1)\}\right\}^{\frac{1}{2}}, \tag{24}$$

where $\alpha'=T/\tau_1$, and $\beta'=K'''/K''$

In the above calculation the constant τ_1 is assumed to be far greater that the constant τ_2, as mentioned above.

The first factor on the right side of the above equation is a constant which is a little different from that of eq. (18), but the form of the equation is almost identical, and the curves for eq. (24) should also be analogous to those for eq. (18), and therefore have been omitted in this paper.

From the above consideration, it may be concluded that the method of voltage pulse makes the accuracy of measurement and also the sensitivity of the device fairly higher than with that of constant voltage.

As another example of the application of the above principle, the following case will be discussed. Assume that we attempt to measure the intensity of a constant light with a multiplier phototube and an a.c. amplifier. The light beam will be chopped before being projected onto the photo-cathode as in the ordinary case. If the amplifier has a very narrow pass-band tuned to the chopping frequency as in the ordinary case, only the fundamental component of the signal will appear in the output circuit. But if we use a wide-band amplifier, the output will contain almost all components of the Fourier series of the input signal. In order to reduce the noise which may also appear in the output, a synchronous rectifying system could be adopted, and this reduces only the noise without affecting the signal intensity in the output. Moreover, the noise voltage due to

* K''/K''' has the same meaning as n_s/n_d in the previous case of the constant voltage method.

the dark current in the multiplier phototube, which is the main part of the noise as mentioned above, could be reduced down to half of the initial value by the above-mentioned pulse voltage method. Thus the ratio (S/N) would increase up to $\pi/\sqrt{2}$ of that in the ordinary method. Therefore the accuracy of measurement will increase by $\pi/\sqrt{2}$ and also especially in case of an automatic recording system, the time necessary for the recording will be reduced by $2/\pi^2$ as compared with that of the ordinary system.

3. Summary

The author has theoretically discussed the photoelectric measurement of the spectrum line intensity with the combination of a phototube and a.c. amplifier and also with a multiplier phototube.

It is shown that the multiplier phototube has, in general, a higher sensitivity than the combination of a phototube and a.c. amplifier.

The difference in sensitivity is especially marked in the case where the intensity of a periodically pulsating light must be measured.

Since in this case the sensitivity of the multiplier phototube can easily be made null during the interval of time when no signal light is projected onto the photo-cathode, the dark current, which is the main part of the noise, can also be suppressed during the same interval. Therefore the accuracy could be increased by eliminating the main part of the error, and thus the sensitivity could also be made so much higher than with constant voltage.

The author wishes to express his appreciation to Dr. H. Yoshinaga for his many instructive suggestions, Mr. S. Minami for his valuable assistance and also wishes to thank Dr. Y. Uchida for his kind encouragement in this study. In addition the author wishes to acknowledge the support of this study by the Grant in Aid for Fundamental Research of the Ministry of Education of the Japanese Government.

The Band Spectrum of Nitric Oxide in the Near Infrared Region.

Masaru OGAWA

Institute for Optical Research, Tokyo University of Education.

(Received August 31, 1953)

Emission bands of NO in the near infrared region were photographed, using electrical excitation of flowing NO gas at relatively high pressure. Vibrational analysis was made tentatively for the complex bands of around 8,600, 7,800, and 7,250 A. Considering the experimental conditions and comparing electron configurations of O_2^+ with possible electronic states of NO built up from separate atoms having given terms, it was concluded that these bands seem to belong to a single system ($^4\Sigma^- - {}^4\Pi$) of NO predicted by Mulliken.

1. Introduction

Electronic states of nitric oxide have been studied by many authors and many doublet states have been observed. It is very remarkable that the states with higher multiplicity than the doublet have not yet been observed, although in the O_2^+ molecule which is isoelectronic with NO, $^4\Sigma_u^-$ and $^4\Pi_g$ states have been observed, in the first negative bands. R. S. Mulliken[1] discussed theoretically the electronic states of NO. According to his argument, it may be expected that the $^4\Sigma^- - {}^4\Pi$ transition will appear in the emission spectrum of NO.

In order to detect this $^4\Pi$ state, L. G. Mundie[2] tried the observation of an absorption spectrum due to the forbidden transition ($^4\Pi \leftarrow X^2\Pi$), using a long absorbing path of 6 meters, but he was not successful. G. Herzberg and H. J. Bernstein[3] also tried the same experiment through a path length of 30 meters and under relatively high pressure ranging from 75 to 700 mm Hg, but they could not observe the band. Recently, M. W. Feast[4] observed the complex bands of NO which resemble the first negative bands of O_2^+, around 8,600 and 7,800 A when the flowing NO_2 gas was activated by silent discharge.

As reported in a previous paper,[5] the same bands were observed by the author when silent discharge was applied to the flowing NO gas under a pressure

1) R. S. Mulliken: Rev. Mod. Phys., **4** (1932) 51.
2) L. G. Mundie: M. A. Thesis, Univ. of Saskatchewan, (1937).
3) G. Herzberg and H. J. Bernstein: Jour. Chem. Phys., **15** (1947) 77.
4) M. W. Feast: Canadian Jour. Res., **28** (1950) 488.
5) M. Ogawa: Science of Light, Tokyo, **2** (1953) 87.

of a few mm Hg. No vibrational analysis has yet been tried for these bands. To perform the analysis, it is necessary to find out at least three bands belonging to one progression. Unfortunately, the bands observed seem to belong only to two sequences, or to groups of two bands of one progression. Therefore, our purpose was to find out other sequences and thus to complete the vibrational analysis. For this purpose an emission spectrum of NO in the near infrared region was photographed under electrical excitation of flowing NO gas. Besides the bands above mentioned other weak bands resembling them were observed around 7,250 A.

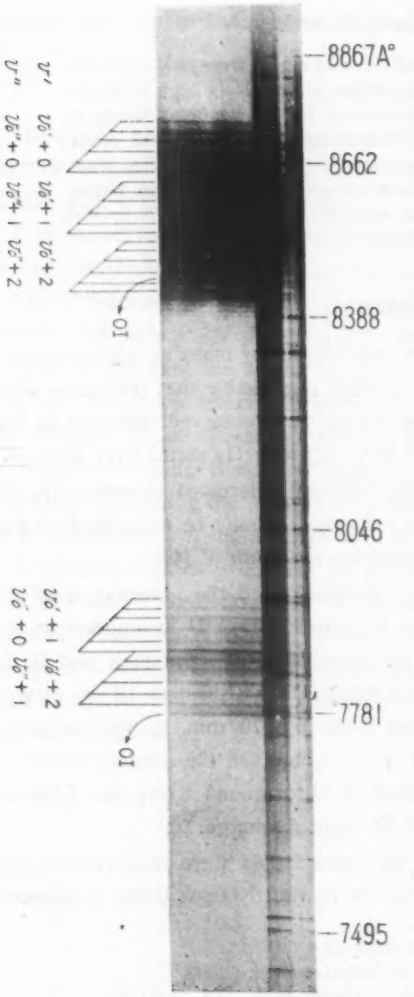

Plate 1. Spectrum of Nitric Oxide in the Near Infrared Region.

Vibrational analysis was made for these complex bands. Comparing the energy of excitation incurred predominantly under the present experimental conditions with that of the electronic states of NO^+, or with that of the electronic states of NO having high multiplicity, it was concluded that the bands in question seem to belong to a single system ($^4\Sigma^- - ^4\Pi$) of NO which was predicted by Mulliken.

2. Experiments

The experimental method was the same as in the previous paper. When the pressure of the flowing NO was between 10 and 18 mm Hg, the superposition of the first positive group of N_2 and the continuous spectrum of the air afterglow on the bands around 8,600 and 7,800 A could be avoided, since those bands were strong, as shown in Plate 1. From the intensity distribution of these bands, other sequences expected to exist in the shorter wavelength side was thought to be weak,

so that long exposure times seemed to be called for to photograph them. Under these circumstances, the superposition of the first positive group of N_2 and the continuous spectrum on the weak band became unavoidable. Therefore, a sector, reported in the previous paper was used to avoid it. NO gas at about five mm Hg was used in order to economize the gas, since longer exposure times were needed in this case. In spite of this method, the first positive group and continuous spectrum were not completely excluded, but very weak bands could be observed of about 7,250 A which had nearly the same appearance as that of the above mentioned strong bands on the longer wavelength side. The photographic plate used was Kodak 1-N. The exposure times to photograph the strong and the weak bands were about 3–10 minutes and 2–4 hours respectively.

3. Vibrational Analysis

The bands around 8,600, 7,800 and 7,250 A are groups of band heads and each band degrades to the shorter wavelength side. The structures of these groups are complex but their appearances are very similar to each other. Hence, it was considered that each of these groups is a sequence belonging to a single band system. Numbers of the heads of each group are 18, 12 and 6 counting from the longer wavelength side. From the appearance of the bands and the numbers of the heads, it may be considered that the six heads belong to one band corresponding to a given $v'-v''$ transition. Among these six heads the third one from the longer wavelength side is rather stronger and more diffuse than the others and the fourth one also relatively strong.

Vibrational analysis was made for these complex bands. The wavenumbers of the heads obtained from this analysis can be shown by the following formula,

$$\nu_{v_0'+n',\ v_0''+n''} = \left.\begin{matrix}11{,}378\\11{,}401\\11{,}424\\11{,}452\\11{,}480\\11{,}503\end{matrix}\right\} +1{,}168.0(n'+1/2)-13.3(n'+1/2)^2 \\ -1{,}019.0(n''+1/2)+12.8(n''+1/2)^2. \qquad (1)$$

Since no sequences corresponding to negative Δv values could be observed, it was impossible to determine the correct v values. Thus $v_0'+n'$ and $v_0''+n''$ respectively were used instead of v' and v''. The wavenumbers of the band heads calculated according to the above formula, and observed, are listed in Table 1. Deslandre's table is shown in Table 2.

4. Discussions of the Results.

When an electric discharge was applied to NO under a pressure below 1 mm

Table 1

v' v''	λ observed (in A)	ν observed (in cm^{-1})	ν calculated (in cm^{-1})	v' v''	λ observed (in Å)	ν observed (in cm^{-1})	ν calculated (in cm^{-1})
	8730.6	11451	11453		7936.2	12597	12596
	8710.7	11477	11476		7922.3	12619	12619
$v_0'+0$,	8695.1	11498	11499	$v_0'+1$,	7908.6	12641	12642
$v_0''+0$	8672.8	11527	11527	$v_0''+0$	7890.9	12669	12670
	8651.8	11555	11555		7874.5	12696	12698
	8636.4	11577	11578		7860.0	12719	12721
	8616.9	11602	11602		7860.0	12719	12717
	8597.9	11628	11625		7846.9	12740	12740
$v_0'+1$,	8584.1	11646	11648	$v_0'+2$,	7833.3	12762	12763
$v_0''+1$	8560.5	11678	11676	$v_0''+1$	7815.7	12791	12791
	8541.8	11704	11704		7798.4	12820	12819
	8525.7	11726	11727		7787.3	12844	12842
	8509.2	11749	11749		7291.5	13711	13711
	8493.2	11771	11771		7279.3	13734	13734
$v_0'+2$,	8474.3	11797	11795	$v_0'+2$,	7266.6	13758	13757
$v_0''+2$	8455.5	11823	11823	$v_0''+0$	7251.8	13786	13785
	8435.5	11851	11851		7236.6	13815	13813
	8423.2	11869	11874		7225.3	13837	13836

Table 2. Deslandres' table (in cm^{-1})

v' \ v''	$v_0''+0$		$v_0''+1$		$v_0''+2$
	11451				
	11477				
$v_0'+0$	11498				
	11527				
	11555				
	11577				
	1146				
	1142				
	1143				
	1142				
	1141				
	1142				
	12597	*995*	11602		
	12619	*991*	11628		
$v_0'+1$	12641	*995*	11646		
	12669	*991*	11678		
	12696	*992*	11704		
	12719	*993*	11726		
	1114		*1117*		
	1115		*1112*		
	1117		*1116*		
	1117		*1113*		
	1119		*1116*		
	1118		*1118*		
	13711	*992*	12719	*970*	11749
	13734	*994*	12740	*969*	11771
$v_0'+2$	13758	*996*	12762	*965*	11797
	13786	*995*	12791	*968*	11823
	13815	*995*	12820	*969*	11851
	13837	*993*	12844	*975*	11869

Hg, only strong N_2 bands were observed in the near infrared and the visible regions. On the other hand, when the pressure of the flowing NO was increased to several mm Hg the N_2 bands disappeared and instead the bands in question as well as the E−A, B′−B and B″−B bands of NO became bright. Hence, it seems probable that the bands in question originate from either NO or NO^+.

Recently, E. Miescher and P. Baer,[6] and Y. Tanaka[7] observed the emission spectrum of $NO^+(^1\Pi-X^1\Sigma)$ in the far ultraviolet region and Tanaka performed vibrational analysis thereof. The vibrational constants shown in the formula of the present paper do not agree with any given by Tanaka. In another report Tanaka[8] has suggested the values for ν_{00} of the $^1?-X^1\Sigma$ and the $^3\Pi-^3\Sigma$ systems of NO^+, calculated from the series limits of three Rydberg series observed by him and the first ionization potential of NO. No bands observed in the present work agree with these ν_{00} values. It is seen from the appearance of the bands shown in Plate 1, that the bands correspond to the transition between triplet states or between states with higher multiplicity, if the bands are attributed to the NO^+ molecule; while the excitation energies of the first and second excited triplet states of NO^+ (the series limits of β- and γ-Rydberg series of Tanaka) are 15.6 and 18.2 eV respectively. All known bands of NO observed in the present work correspond to excitation energies below 8 eV and were taken at a relatively high pressure. Therefore, it is unlikely that direct electrical excitation above 18 eV should have been predominant, or that numerous NO^+ have been produced and excited. From the above considerations, it might be concluded that the bands in question arise from NO (neutral molecules).

Many states are known of atomic oxygen and nitrogen, among which are also found many, the combinations of which give quartet or sextet electronic states of NO. The bands observed can be explained as bands due to the transition between quartet or sextet states if the heads correspond P and Q, or P heads respectively. In this case, the correlation between the heads and the sublevels may be represented by the following figures.

Transition between sextet states.

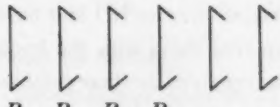

Transition between quartet states

6) E. Miescher and P. Baer: Nature, **169** (1952) 58.
7) Y. Tanaka: J. Chem. Phys., **21** (1953) 562.
8) Y. Tanaka: Sci. Paper I. P. C. R. (Tokyo), **39** (1942) 456.

As mentioned above, NO is isoelectronic with O_2^+ and good correspondence has been recorded between two in regard to the results of experimental observations and from the standpoint of considerations concerning electron configurations. Therefore, it may be reasonable to consider in analogy the electron configurations of O_2^+ which lend themselves to the production of sextet states. In Table 3 are shown those configurations having relatively low excitation energies. An electron configuration of the ground state of O_2^+ is also tabulated. Comparing the configurations of the sextet states with that of the ground state, it is seen that these sextet states are very highly excited. From considerations on the stability of the known states of O_2^+ and NO, it may be said that all the electronic states shown in Table 3 except the ground state are either unstable or have dissociation energies below a few electron volts.

Table 3. Electron configurations of O_2^+ molecule, which are possible to produce the sextet states.

$\sigma_g 2p$	$\pi_u 2p$	$\pi_g 2p$	$\sigma_u 2p$	$\sigma_g 3s$	$b-a$*	Molecular States
2	4	1			5	$^2\Pi$(ground state)
2	2	2	1		1	$^6\Sigma^+$
2	2	2		1	3	$^6\Sigma^+$
2	2	1	1	1	3	$^6\Pi$
2	1	2	1	1	1	$^6\Pi$
1	3	2	1		1	$^6\Pi$
1	3	2		1	3	$^6\Pi$
1	2	3	1		−1	$^6\Pi$
1	2	3		1	1	$^6\Pi$
1	3	1	1	1	3	$^6\Sigma^+$ $^6\Sigma^-$ $^6\Delta$

* b and a are the numbers of the bonding and antibonding electrons respectively, σ_g and π_u electrons are bonding and π_g and σ_u electrons are antibonding.

The combinations of atomic states which lend themselves to the building up the sextet states of NO and have relatively low term values are shown in Fig. 1. Comparing these with the known excited states of NO, the excitation energies of the states given by these combinations are deemed to be very high. The $^6\Sigma^+$ state built up from both normal states corresponds to the configuration in the second line of Table 3 and is unstable. The lowest term value of the separate atoms, excepting that of the normal atoms, is as high as 14.4 eV or 15.1 eV)[9] from the

9) According to Gaydon, D_0(NO) is 6.48 eV. A. G. Gaydon: *Dissociation Energies*, (London): Chapman and Hall, 1947.

ground state. Considerations on the dissociation energies of the case of O_2^+ indicate that the dissociation energies of the stable sextet states of NO might be below a few electron volts. Therefore, in order to find strong bands in the near infrared region, an excitation as high as above 14 (or 15) eV must occur predominantly. As above mentioned, it might be difficult to presume the occurrence of such a high excitation process in the present experiment.

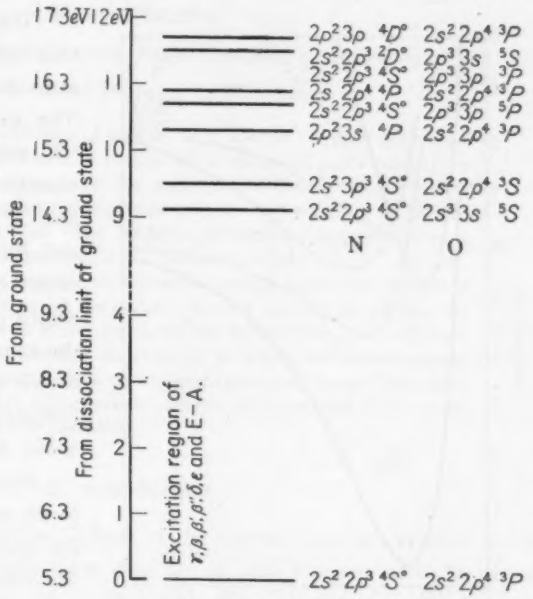

Fig. 1

As described in paragraph I, Mulliken predicted the existence of the stable $^4\Sigma^-$ and $^4\Pi$ states built up from combinations of separate atoms $2s^2\ 2p^3 N(^4S) + 2s^2\ 2p^4\ O(^1D)$ and $2s^2\ 2p^3 N(^4S) + 2s^2\ 2p^4\ O(^3P)$ and respectively having the electron configurations $\sigma\pi^4\pi^2$ and $\sigma^2\pi^3\pi^2$. The potential curves of NO given by him are shown in Fig. 2. The curves show that the molecular constants of these two states resemble that of the corresponding states of O_2^+, and the excitation energy of the $^4\Sigma^-$ is below 8 eV. The vibrational constants of the bands observed are nearly the same as those of O_2^+:

$$\omega_e' = 1196.77 \quad \omega_e'x_e' = 17.09 \quad \omega_e' = 1035.69 \quad \omega_e''x_e'' = 10.39 \quad \text{for } O_2^+$$
$$(\omega_e') = 1168.0 \quad (\omega_e'x_e') = 13.3 \quad (\omega_e'') = 1019.0 \quad (\omega_e''x_e'') = 12.8 \quad \text{for NO.}$$

These facts suggest that these are the bands predicted by Mulliken.

The dissociation energies calculated from the relation $D_e = \omega_e^2/4\omega_e x_e$ are 24,758 cm^{-1} for the upper and 20,280 cm^{-1} for the lower state, assuming that the above constants for NO accord with the true values. It is well known that a dissociation energy calculated from this relation comes out greater than the actual value. But these two values for NO are nearly equal. Therefore, it might be considered that the differences between these and the actual values are also nearly equal,

and a value calculated according to the relation $D_e'+\nu_e-D_e''$ should show approximately, the energy difference of the separate atoms. The value obtained according to this relation 15,894 cm^{-1} which almost agrees with the difference between the term values of $O(^1D)$ and $O(^3P)$, that is, 15,870 cm^{-1}.

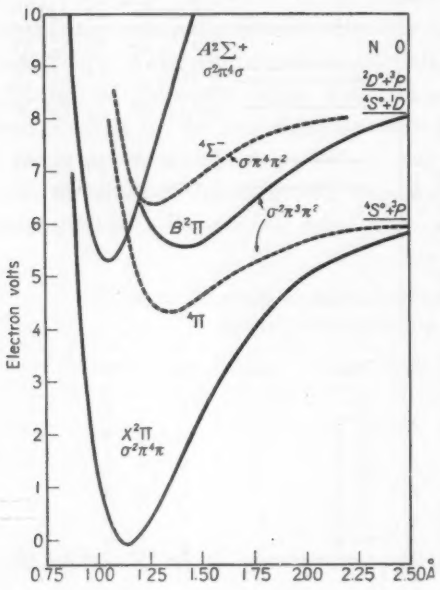

Fig. 2

The states with the same electron configuration have nearly the same values of molecular constant. The molecular constants of the $A\,^2\Pi_u$ and $a^4\Pi_u$ states of O_2^+ are an example of this, as also $b^1\Sigma_g^+$, $a^1\Delta_g$ and $X^3\Sigma_g^+$ states of O_2, and $a^1\Pi_g$ and $B^3\Pi_g$ states of N_2. The molecular constants of the lower state shown in the formula 1 are nearly the same as that of the $B^2\Pi$ state of NO which has the same electron configuration ($\sigma^2\pi^3\pi^2$) as that of the above mentioned $^4\Pi$ state.

From above discussions, the bands analyzed seem to arise from the transition $^4\Sigma^- - ^4\Pi$ predicted by Mulliken, although the following doubts still remain regarding the intensity distribution: The observed intensities of the third and fourth heads should be more intense, though they actually are slightly stronger than the others. Only the bands with $n' \leqq 2$ have been observed in the present experiment. In order to interpret the disappearance of the bands with $n' \geqq 3$, it must be assumed that a forbidden predissociation or some particular excitation process occurs, because the unstable states built up from both the normal states are the $^2\Sigma^+$, $^4\Sigma^+$, $^6\Sigma^+$ and $^6\Pi$ states, all of which can not bring the $^4\Sigma^-$ state to the allowed predissociation.

The author wishes to express his sincere thanks to Professor Yoshio Fujioka, Director of the Institute, for his interest and for valuable discussion upon the present work. He is also much indebted to Professor Yoshio Tanaka for his encouragement and valuable advice in the course of this work and to Professor R. S. Mulliken for his kind and valuable discussion.

On the Origin of Sodium D-lines in the Nightglow and Twilight Flash

Masaru OGAWA

Institute for Optical Research, Tokyo University of Education

(Received February 1, 1954)

The low pressure reactions of sodium with atomic oxygen, molecular oxygen and ozone have been investigated in order to make laboratory check of Chapman's process of the nightglow. Sodium vapor reacts with ozone in the gas phase accompanied only by the emission of D-lines which are slightly diffuse. The velocity of reaction betweem atomic sodium and ozone is larger than that between atomic sodium and molecular oxygen. On the basis of experimental results and in consideration of the dissociation energy of NaO, one plausible process to explain the above chemiluminescence is set forth, which differs from that of Chapman. It is impossible, however, to attempt to attribute to this process the origin of the sodium D-lines in the nightglow and the twilight flash in the upper atmosphere. Chapman's process would appear to be endothermic and therefore not plausible.

1. Introduction

It is well known that diffuse D-lines of the sodium atom are emitted in the nightglow, and in the twilight these lines are of such intensity as to be named flash. The intensities are 8×10^7 photons/cm^2. column. sec in the nightglow and 1.5×10^{10} in the twilight flash.

R. Pendorf[1] has proposed the following reaction process to describe the emission mechanism of sodium D-lines in the twilight flash,

$$Na+N_2O \rightarrow NaO+N_2+1.32\,ev \qquad (1)$$

$$NaO+Na_2 \rightarrow Na_2O+Na(^2P)+0.84\,ev \qquad (2)$$

$$Na(^2P) \rightarrow Na(^2S)+h\nu(5{,}890\,A). \qquad (3)$$

He determined these reactions from the experimental results obtained in the labolatory by C. E. H. Bawn and A. G. Evans[2], and further assumed the photodissociation of Na_2O along the following pattern:

$$Na_2O+h\nu(\lambda\leq2{,}031\,A) \rightarrow Na_2+O, \qquad (4)$$

through which are supplied the sodium molecules necessary for the reaction (2).

The sodium monoxide (NaO) concentration necessary to justify the appearance

1) R. Pendorf: Phys. Rev., **78** (1950) 66.

2) C. E. H. Bawn and A. G. Evans: Trans. Farad. Soc., **33** (1937) 1571.

of D-lines in the twilight flash of the intensity of the order of 10^4 photons/cm^3. sec, has been computed by F. D. Kahn[3], who took into account the reaction set forth by R. Pendorf. The result indicates that a concentration adequate to interpret the observed intensity would be impossibly high.

J. Bricard, A. Kastler and R. Robly[4] observed the polarization of the D-lines in the twilight flash and concluded that they were the resonance lines caused by sunlight. The resonance theory has been generally accepted for the interpretation of the emission mechanism of the D-lines in the twilight flash, but their intensity variation observed by L. Vegard and G. Kvifte[5] may hardly be interpreted by this commonly accepted theory.

The most well known process to explain the emission mechanism of D-lines in the nightglow is S. Chapman's[6], that is:

$$Na+O_3 \rightarrow NaO+O_2 \text{ (in the lower level)}, \quad (5)$$

$$Na+O+X \rightarrow NaO+X \text{ (in free atomic oxygen region)}, \quad (6)$$

$$NaO+O \rightarrow Na(^2P)+O_2, \quad (7)$$

$$Na(^2P) \rightarrow Na(^2S)+h\nu. \quad (8)$$

D. R. Bates and Marcel Nicolet[7] studied various plausible reactions under the assumption that the emission of D-lines in the nightglow was directly connected with the atmospheric sodium, and gave the two most probable reactions in altitudes below 100 km*:

$$NaO+O \rightarrow Na(^2P)+O_2, \quad (9)$$

$$NaH+O \rightarrow Na(^2P)+OH. \quad (10)$$

The first reaction is identical with Chapman's (7). The following reaction has been also suggested by D. R. Bates[8]

$$NaH+H \rightarrow Na(^2P)+H_2. \quad (11)$$

The emission mechanisms of the D-lines have important relations with other

3) F. D. Kahn: Phys. Rev., **78** (1950) 167.
4) J. Bricard, A. Kastler and R. Robly: C. R. Acad. Sci. Paris, **228** (1949) 1601.
5) L. Vegard and G. Kvifte: Geophys. Publ., **16** Nr. 7, (1945).
6) S. Chapman: Astrophys. J. 90, (1939) 309.
7) D. R. Bates and M. Nicolet: J. Geophys. Res., **55** (1950) 235.
D. R. Bates and M. Nicolet: J. Geophys. Res., **55** (1950) 301.
D. R. Bates and M. Nicolet: C. R. Acad. Sci., Paris, **230** (1950) 1943.
8) Private communication.

* The height of the emission stratum has been variously estimated. In the case of nightglow, the values differ widely from each other, though the same Van Rhjin's method was used in each case, for example, J. Cavannes, J. Dufay and J. Gauzit had 130 km, J. Dufay and Tcheng Mao-Lin 80 km and F. E. Roach and D. Barbier 250 km. In the case of the twilight flash, the reported values were 60 km according to R. Bernard and 90~105 km according to L. Vegard and G. Kvifte.

various phenomena in the upper atmosphere. An important and interesting question is to confirm these mechanisms in the laboratory. The principal purpose of the present experiment was to perform such laboratory checks of Chapman's process. In order to do this, the reaction of sodium vapor with atomic oxygen, molecular oxygen and ozone were investigated. In section 2, it will be found that sodium vapor react with ozone accompanying only by the emssion of diffuse D-lines. In section 3 will be reported an investigation of the temperature dependence of the intensities of the D-lines and it will be seen that the molecular sodium is a necessary component of the above chemiluminescence. Section 4 reports the study of the reaction of sodium vapor-atomic oxygen and sodium monoxide-atomic oxygen. From the results of these experiments, it may be considered that Chapman's process does not occur. The reaction process of the chemiluminescence was derived from the above experimental results and from a consideration of the dissociation energies of the related components, but the process was found to be different from Chapman's. This is reported in section 5. In section 6, is discussed the possibility of applying the mechanism obtained in the preceding section to the upper atmosphere as an explanation of the origin of D-lines in the nightglow or twilight flash, but the final conclusion is that this mechanism is not applicable.

2. The reaction between sodium vapor and ozone.

The experimental apparatus is shown in Fig. 1. The oxygen was produced by heating potassium-permanganate, and the water vapor therein contained was removed by phosphoric oxide (P_2O_5). The ozonizer tube was 50 cm long and its inner diameter was 7 mm. Four aluminum foils surrounding the tube and 10 cm apart were used as electrodes for the ozonizer. The electric source was a transformer of 20 KV, 0.3 KVA capacity. The reaction tube was made of Hirom-glass with a dimension of 23 cm long by 13 mm inner diameter.

The sodium was vaporized and introduced into the reaction tube by heating the distillation tube with a Bunsen flame. The ozonizer tube was filled with oxygen to a pressure above 50 mm Hg. An electric discharge was applied to this gas, and then the gas was passed through the reaction tube, and it was found that the gas reacted with the sodium vapor, emitting the light characteristic of sodium atomic lines. If the discharge was stopped, this emission continued for about one minute or more. This light became very weak when the pressure in the ozonizer was reduced to below 2 mm Hg, which is equal to that in the reaction tube. When the discharge was stopped, however, this glow died out immediately. In either case the glow of so-called stray discharge was observed

in the tube between the ozonizer and the reaction tube. But in the case where the pressure in the ozonizer tube was higher, the intensity of the glow in the reaction tube was stronger and was accompanied by after-glow. It may therefore be assumed that the glow is associated with the gas activated by the ozonizer discharge at higher pressure.

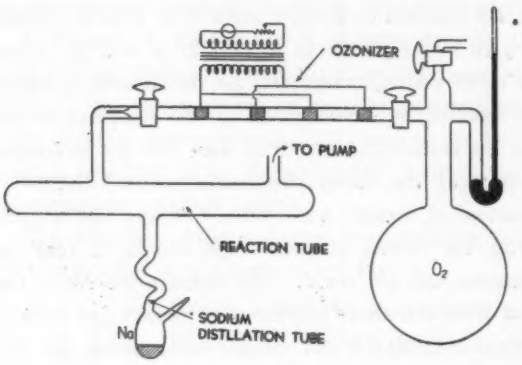

Fig. 1

Since the possibility of generation of ozone in the ozonizer is high in the case of the higher pressure, the above preliminary experiments suggest that ozone reacts with the sodium vapor and that this reaction is accompanied by the glow characteristic of sodium atomic lines.

To ascertain that the light was not emitted by stray discharge or by the reaction of sodium with some elements in the gas besides ozone, the gas affected by the electric discharge was preserved in a flask with a capacity of 3-liters and was used again after an interval of two hours: the glow was still observed. This shows clearly that the glow originates from the reaction between sodium vapor and ozone.

Pure ozone gas was prepared by evaporating liquid ozone. When this gas was led into the reaction tube, the glow was extremely strong. In this case the reaction was so violent that if the gas flowed in at a comparatively high pressure, the reaction was immediately completed, changing the sodium into a white compound which was deposited on the wall of the reaction tube. The pressure of ozone enough to cause a continuing glow at a suitadle intensity was so low as to be impossible to measure by the U type mercury manometer used.

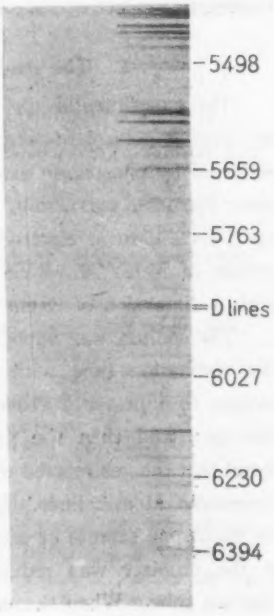

Plate

The spectrum of this glow was photographed by two spectrographs, the one composed of two 60° glass prisms, with a dispersion of 79 A/mm at region near 5,900 A and with a slit width of 0.025 mm, while the other was a Hilger E_6 quartz spectrograph. The spectrum photographed by the former is shown in Plate 1. Both this and another plate obtained by the E_6 show only D-lines which are slightly diffuse.

Since the reaction between sodium and pure ozone is very violent, the experimental procedure must be carried out very carefully. On the other hand it is difficult to cause sodium to react upon oxygen molecule at such a rate as to emit light. For above two reasons oxygen only partly ozonized was used instead of pure ozone. Special precautions were taken to prevent the entering of stray discharge into the reaction tube. The ozonizer tube was replaced by the one shown in Fig. 2, and the tube between the ozonizer and the reaction tube was lengthened to about 1.5 meters, and an earthed aluminum foil was rolled around it at a point

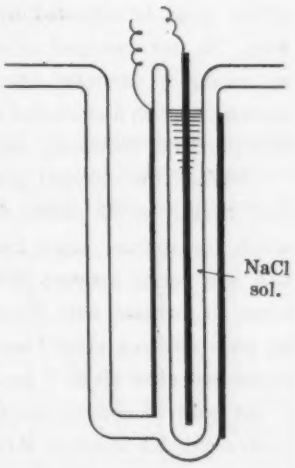

Fig. 2

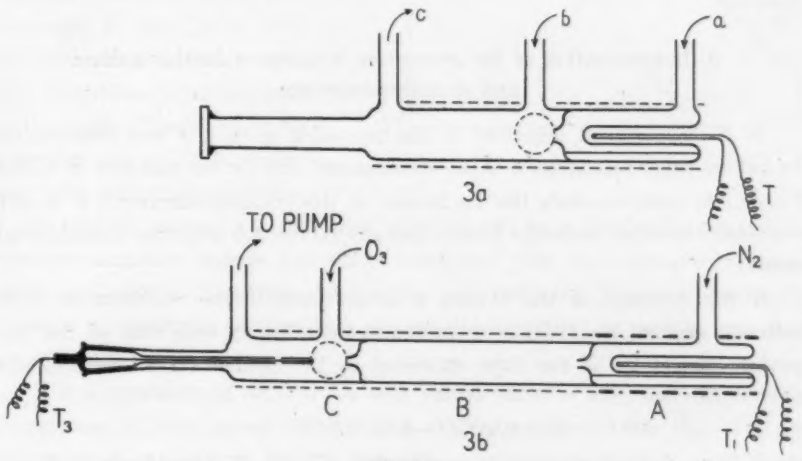

Fig. 3

immediately before the reaction tube. In this way it was assured that no stray discharge entered into the reaction tube. The reaction tube shown in Fig. 3a

was used in order to provide for adjustment of the temperature of the sodium tank and the reaction zone. The tank, with an inner diameter of 20 mm and a length of 50 mm, had a covering of asbestos in which was embedded a coil of Ni–Cr wire. The thermometer T measured the temperature in the sodium tank, which could be adjusted by controlling the current flowing through the Ni-Cr wire. N_2 gas was used as carrier gas of sodium vapor. The gas was prepared by adding a saturated aqueous solution of $(NH_4)_2SO_4$ into a saturated $NaNO_2$ aqueous solution and washed by passing it through conc H_2SO_4 and through grain KOH, and the remaining water vapor was removed by P_2O_5.

When the ozonized gas was led into the reaction tube from the upper gas inlet, a glow of the candle flame type was observed in front of the nozzle from which the sodium vapor came into the reaction zone. The temperature of the tank was varied between 200° and 500°C, and the intensity of the glow was found to increase with temperature. When the electric discharge was stopped, the glow died out after 7 seconds. Upon resumption of the discharge, the glow reappeared after about 7 seconds.

In order to observe spectra other than the D-lines, another spectrograph was constructed, the aperture ratio of which (f=3.5) is larger than that of the two spectrographs above mentioned. The spectra of the glow was photographed with this spectrograph with a 30 minute exposure but the other spectra could not be observed.

3. Determination of the connection between molecular sodium and chemiluminescence.

In the experiment described in the preceding section, it was observed that the sodium vapor reacted with ozone, accompanied only by the emission of sodium D-lines. In order to study the mechanism of this chemiluminescence, it must be determined whether molecular sodium had any connection with the chemiluminescence.

If the intensity of the D-lines is proportional to the concentration of the molecular sodium, the relation of change of the intensity with that of the temperature should be of the form expressed by the formula (27) in the appendix, that is,

$$(\log I/I_0)/(1/T-1/T_0)=D/R \qquad (12)$$

where I and I_0 are intensities at temperature T and T_0 respectively and D is dissociation energy of the sodium molecule. The $\log I/I_0$ curves are shown in Fig. 4. If the presence of molecular sodium is necessary for the emission of the D-lines, it may be expected from this figure that the intensity of the D-lines

would decrease with increase the temperature of the reaction zone. Such reaction are quite common to us, an example being the reaction of sodium with halogen gas. Taking as an instance the reaction of sodium with chlorine, the D-lines are emitted according to the following process

$$\begin{aligned} &Na+Cl_2 \rightarrow NaCl+Cl \\ &Na_2+Cl \rightarrow Na(^2P)+NaCl \\ &Na(^2P) \rightarrow Na(^2S)+h\nu. \end{aligned} \tag{13}$$

H. Ootsuka[9] determined the $D(Na_2)$ from the change of the luminescence intensity with the temperature in the reaction zone for the case of sodium vapor and bromine, and the resulting value of 19 Kcal agrees fairly well with more recent value. This fact should be considered to prove that this form of experiment is justified for determining the connection between molecular sodium and luminescence.

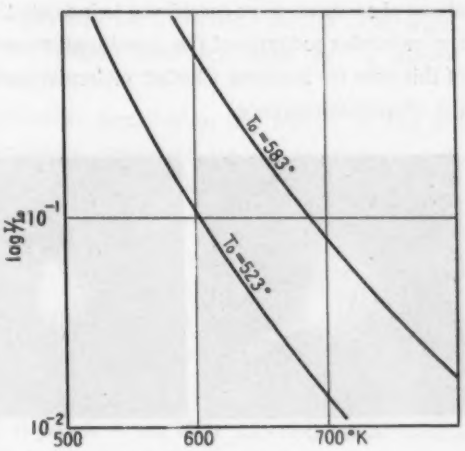

Fig. 4

The reaction tube shown in Fig. 3b was used. The sodium tank A was 16 cm long with an inner diameter of 20 mm. The part B was 16 cm long, and this part and the reaction zone were heated simultaneously by the method described in the preceding section. The sodium tank being heated independently. It was deemed necessary to prove that this form of tube is suitable for determining whether molecular sodium has many connection with this chemiluminescence, and so the reaction of sodium and chlorine was first tried, in which reaction the presence of molecular sodium is a prerequisite ingredient as may be seen from the formula (13).

The temperature of the Part A was varied between 250° and 350°C. The carrier gas N_2 was passed through it at a pressure below 1 mm Hg. The concentration of the sodium carried into the reaction zone through part B was considered to be constant, since the temperature of part A (sodium tank) was controlled to stay. The reaction zone, observable through a side window, was

9) H. Ootsuka: Zeits. f. Phys. Chem., **7** (1930) 407.

irradiated through an opposite window by a sodium resonance lamp the light of which was rendered pararel by being passed through a lens. The reaction zone was dark since the light which comes from the resonance lamp was absorbed by the sodium atoms being carried by the N_2 gas. When chlorine gas was introduced at a pressure below 1 mm Hg from the upper gas inlet, a glow of the candle flame type was seen. The figure of the flame was determined according to the ratio between the quantities of chlorine and sodium. If the portion of the former was reduced, the flame changed from the candle flame type to the sphere or to the cloud type seen in the lower part of the upper gas inlet. When the temperatures of both part B and the reaction zone were increased to 450°C, the part of the flame which emits the characteristic sodium light became very weak. The above phenomena were considered to indicate the existence of connections between the molecular sodium and the chemiluminescence, there by justifying the utilization of this tube for studying whether molecular sodium is necessary or not for causing the chemiluminescence.

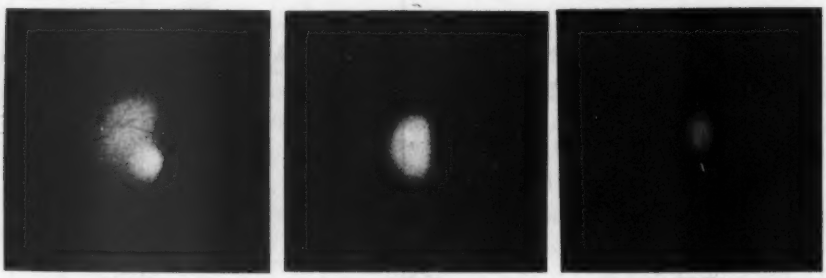

Fig. 5 Appearance of the flame in the reaction of sodium with ozone. Temperature of sodium tank is 300°C.

Next, instead of chlorine, the ozone liquidized by cooling with liquid air and then reevaporated was used, and the temperature of the sodium tank A was fixed at 250° or 300°C and the temperature of reaction zone was varied between 250°~450°C or 300°~450°C. When the ozone was led into the reaction zone, the characteristic sodium light of the usual flame type was emitted, which became smaller and the intensity weaker as the temperature of reaction zone was increased. The light almost died out at 450°C in both cases. In Fig. 5, is seen the appearance of the flame photographed through the side window. In this case the oxygen led through the ozonizer was used, and the concentration of the ozone contained was relatively low, making it necessary to increase the pressure of the ozonized gas to about 2 mm Hg, so that the pressure of the carrier gas had to be relatively

high and the sodium vapor carried through in a unit time large. For this reason, the light did not die out completely at 450°C.

When the ozone was used immediately after reevaporation and the reaction zone irradiated by the sodium resonance lamp, the outside of the flame was bright, but this became dark as time passed. This shows that the atomic sodium which absorbs the light coming from the resonance lamp does not exist outside the flame immediately after the reevaporation of ozone. When light was emitted by the reaction, the temperature of the reaction zone increased by about 7°C. The magnitude of this increase depended on the conditions of the experiment, especially on the distance between the thermometer and the light flame. When only oxygen was led into the reaction zone at the same pressure as that of the ozonized oxygen the emission of light was not observed. In this case, when the reaction zone was irradiated by the sodium resonance lamp only a shadow of the candle flame type was observed.

From the results of the experiments described in this section, it may be said that 1) molecular sodium is a necessary ingredient for the production of luminescence in the sodium vapor-ozone reaction, 2) sodium vapor reacts with molecular oxygen but does not emit light, and 3) the reaction velocity of ozone and atomic sodium is larger than that of molecular oxygen and atomic sodium*.

4. Chapman's mechanism and the reaction between sodium vapor and atomic oxygen-molecular oxygen mixture.

As will be seen in the next section, the sodium atom reacts with ozone and changes into NaO. If $D(NaO)$ is below 4 ev, NaO will decrease according to the following reaction, $NaO+Na_2 \rightarrow Na(^2P)+Na_2O$. But the concentration of molecular sodium is about 1/100 of that of atomic sodium as shown in Fig. 8, so that the decrease of NaO is very small and a comparatively large portion of the NaO might remain around the top of the flame. If Chapman's mechanism is true and atomic oxygen is induced toward the top of the flame, light may be expected to be emitted.

In order to check Chapman's mechanism, the tube shown in Fig. 6 was used. Part A (the sodium tank) was 25 mm in inner diameter and the distance between nozzle a and b could be varied from 15 mm to 25 mm by rotating tube B. The discharge tube B was of water cooled type with an inner tube of 3 mm diameter

* F. Haber and H. Sachasse have been studied the reaction between sodium vapor and molecular oxygen and have obtained the following process $Na+O_2+X \rightarrow NaO_2+X$, $NaO_2+Na \rightarrow 2NaO$, together with the reaction velocity of the former. (Zeits. f. Phys. Chem. Bodenstein-Festband, (1931) 881.)

and 18 cm long. As electric source a 1 KVA, 30 KV transformer was used. The temperature of the sodium tank was controlled in the range of 300°~350°C. When the ozonized oxygen was led into the reaction zone from the gas inlet a the characteristic sodium light of candle flame type was seen, and this flame was adjusted to reach the nozzle b by adjusting the flow of the ozonized gas or the carrier gas and by rotating tube B. When the light was produced by this reaction, the condition of the flame did not change even if the ozonized gas was led into the reaction zone from nozzle b and discharged through tube B.

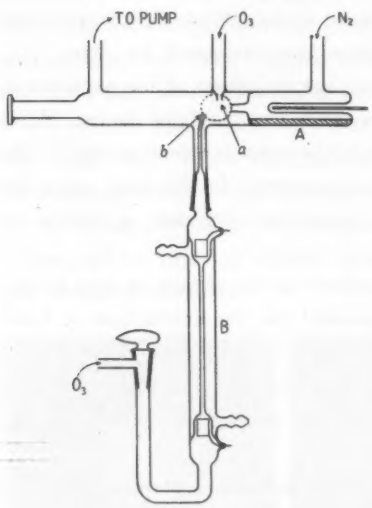

Fig. 6

Hitherto it was considered by many authors that atomic oxygen is a necessary ingredient for the production of air afterglow. Y. Tanaka and M. Shimazu[10] have reported the reaction of nitric oxide and ozone accompanied by a red colored luminescence, which changes into a greenish yellow if the electric discharge is passed through the ozone before the reaction, which color is the same as that of ordinary air afterglow and of which the spectra are also identical. From this experiment the authors have concluded that the components of air afterglow are NO and either atomic oxygen or excited O_2, probably the former. A. G. Gaydon[11] has used this reaction to determine the existence of atomic oxygen in carbon monoxide and other flames.

Therefore, in order to determine whether atomic oxygen reaches the reaction zone from tube B, the following experiment was tried. When NO gas and ozonized gas were led into the reaction zone from inlets a and b respectively unaccompanied by the flow of the carrier gas N_2, a red flame was seen at the upper portion of nozzle b. If an electric discharge was passed through the gas flowing through the tube B the red colored luminescence changed into the greenish yellow light of ordinary air afterglow. Therefore in the case of sodium-ozonized gas reaction, it may be said that the electric discharge through the ozonized gas in tube B always caused atomic oxygen to reach the reaction zone.

10) Y. Tanaka and M. Shimazu: J. Sci. Res. Insti. (Tokyo), **43** (1949) 9.
11) A. G. Gaydon: Proc. Roy. Soc., **183** (1944) 111.

From the results of the experiment above described, it may be said that Chapman's mechanism is endothermic and does not occur.

When the ozonized gas was led into the reaction zone through tube B, light was emitted upwards from the nozzle b. When an electric discharge was passed through this ozonized gas flowing through tube B the chemiluminescence died out. This shows that the reaction of sodium vapor and a mixture of atomic oxygen and molecular oxygen is not accompanied by luminescence.

5. The mechanism of the luminescence in the sodium vapor-ozone reaction.

Before discussing the mechanism of chemiluminescence in the sodium vapor-ozone reaction, the experimental results may be summerized as follows:

1. Ozone reacts with sodium vapor accompanied by the emission of D-lines only.

2. The intensity increases with increase of the temperature of the sodium tank and with decrease of that of the reaction zone. While as seen in Figs. 4 and 8, the increase of the temperature of the sodium tank signifies any increase of the density of both molecular and atomic sodium, the increase of that of the reaction zone means a decrease of molecular sodium. Therefore, it might be concluded that the reaction occurs in the gas phase and molecular sodium is a necessary ingredient of chemiluminescence.

3. The D-lines are slightly diffuse. This is clear, from a comparison in Plate 1 of the D-lines with those in the Fe-arc spectrum shown as reference spectrum.

4. The reaction velocity of atomic sodium and ozone is larger than that of atomic sodium and molecular oxygen.

5. Low pressure reaction of sodium and molecular oxygen or the mixture of atomic oxygen and molecular oxygen is not accompanied by luminescence.

6. The carrier gas N_2 is not a necessary third body in the emission mechanism of the sodium vapor-ozone reaction.

If the mechanism of the chemiluminescence is considered only on the basis of reaction energy, several reaction become plausible as shown in a previous paper[12]. But given the condition that the reaction must satisfy the experimental results described above, and further, eliminating endothermic reactions, our choice of possible reactions is considerable narrowed down. Even there, the determination of the mechnism is difficult, because the correct dissociation energy of NaO which

12) Y. Tanaka and M. Ogawa: Science of Light (Tokyo), **1** (1951) 61.

plays an important role in the mechanism has not yet been definitely determined. C. E. H. Bawn and A. G. Evans[2] obtained 72 Kcal (3.1 ev) as the minimum value of D(NaO) based on the heat of formation in the sodium vapor-NO_2 reaction and on Pauling's approximation rule on the dissociation energy. S. Chapman[6] obtained 4.8 ev as the maximum value from an analogy between the molecular structures of NaO and of OH. Therefore D(NaO) may be thought to be between 4.8 and 3.1 ev.

The reactions which may be considered as plausible on the basis of the experimental results and of the dissociation energies, $D(NaO)=4.8\sim3.1$ ev, $D(Na_2)=0.76$ ev, $D(O_2)=5.09$ ev, $D(Na_2O)=6.1$ ev, $O_3=O_2+O+1.07$ ev, are the following;

$$Na_2+O_3 \rightarrow Na_2O'+O_2 \tag{14}$$

$$Na_2O' \rightarrow NaO+Na(^2P) \quad \begin{matrix}+0.87\,\text{ev}^*\\+0.07\\-0.83\end{matrix} \tag{15}$$

$$Na+O_3 \rightarrow NaO+O_2 \quad \begin{matrix}+3.73\\+2.97\\+2.03\end{matrix} \tag{16}$$

$$Na_2+NaO \rightarrow Na_2O'+Na \tag{17}$$

$$Na_2O'+Na \rightarrow Na_2O+Na(^2P) \quad \begin{matrix}-0.80\\+0.00\\+0.90\end{matrix} \tag{18}$$

or
$$Na_2+NaO \rightarrow Na_2O+Na(^2P) \quad \begin{matrix}-0.80\\+0.00\\+0.90\end{matrix} \tag{19}$$

$$Na(^2P) \rightarrow Na(^2S)+h\nu. \tag{20}$$

Reactions (14) and (15) are plausible from a consideration of enegy, if D(NaO) >3.93 ev, but these reactions are rather speculative since no corresponding electronic state has yet been found. This leaves us with the reactions (16) to (20) a plausible mechanism of the D-line emission in the low pressure reaction of sodium and ozone, the upper limit of D(NaO) being 4.0 ev.

6. Application of the reactions (16) to (20) to the upper atmosphere.

The reactions $NaO+Na_2 \rightarrow Na_2O'+Na$ or $NaO+Na_2 \rightarrow Na_2O+Na(^2P)$ are the same as one of Pendorf's[1], so that the concentration of NaO necessary to explain the intensity of the D-lines in the twilight flash is impossibly high, as has been pointed out by F. D. Kahn[3]. Thus the process cannot be applied to the origin of the D-lines in the twilight flash.

If during day time, the molecular and atomic sodium are in equilibrium according to the processes

* Energies given correspond to D(NaO) of 4.8, 4.0 and 3.1 ev respectively.

$$Na_2+h\nu \rightarrow 2Na \tag{21}$$

$$Na+Na+X \rightarrow Na_2+X, \tag{22}$$

there should exist the relation $[Na_2] \leqq 10^{-12}[Na]^2$,[3] so that [Na] must be larger than $10^{12}/cm^3$ in order that $[Na_2]$ be the same as [Na]. This value of [Na] is impossibly high and consequently $[Na_2]$ must be negligibly small compared to [Na]. If at night molecular sodium is produced by a three body collision process and does not decrease through other reactions, the concentration of molecular sodium may be expressed by the following simple formula,

$$[Na_2]_t = \frac{[Na_2]_{t_0}+\alpha[\times][Na]^2_{t_0}t}{1+2\alpha[\times][Na]_{t_0}t} \tag{23}$$

where α is the reaction coefficient, t the time measured from sunset and $[Na]_{t_0}$ and $[Na_2]_{t_0}$ the concentrations respectively of the atomic and molecular sodium at sunset. If a value of $10^{-30}\,cm^6/sec$ is taken as reaction coefficient α, which is the largest value in three body reaction, and t and $[Na]_{t_0}$ are assumed to be 4.2×10^4 sec and $6\times10^4/cm^3$ respectively, which is very large, $[Na_2]_t$ is found to be less than $6\times10^{-1}/cm^3$ for an altitude of 70~100 km. Of course the observed intensity of the D-lines in the nightglow cannot be explained on the basis of the reactions (16) to (20) and such a value of $[Na_2]_t$. Since this discussion can be applied to any emission mechanism of nightglow involving molecular sodium, it might be said that mechanisms involving molecular sodium are not plausible for explaining the origin of D-lines in the upper atmosphere.

7. Appendix. The equilibrium constant between atomic and molecular sodium.

In the following reaction in the gas phase

$$Na_2 \rightleftarrows Na+Na, \tag{24}$$

the equilibrium constant K_p is defined by $K_p=(P_a)^2/P_m$, where P_a and P_m are partial pressures of atomic and molecular sodium respectively. If the pressure is given in mm Hg, K_p is given by the well known formula

$$\log K_p = \log\frac{(P_a)^2}{P_m} = -\frac{D}{RT}+\log\left\{\mu^{3/2}\frac{\sigma}{10^{40}I}\left(\frac{T}{100}\right)^{3/2}\right\}+\log\left\{1-e^{-\theta_v/T}\right\}$$
$$+\log\frac{v_a^2}{v_m}+13.57 \tag{25}$$

where D: dissociation energy of molecular sodium

μ: reduced mass expressed in atomic weight unit

I: moment of inertia of molecule in g cm^2

θ_v: characteristic temperature related to vibrational frequency in cm^{-1}

σ: symmetry number

v_a, v_m: electronic statistical weights of atom and molecule respectively.

R. Ladenburg and F. Thiele[13] reported the relation between the temperature and the partial pressure of atomic and molecular sodium. Since the correct dissociation energy of molecular sodium $D(Na_2)$ had not been known, they calculated K_p under some assumed valued of $D(Na_2)$ which are higher than more recent values. Today the spectroscopical data necessary to calculate K_p have been precisely determined and K_p has been recalculated on this basis.

If 0.76 ev for $D(Na_2)$ and the spectroscopical data given in the Table of G. Herzberg[14] are used, $\log K_p$ is given by the following formula

$$\log K_p = -\frac{17518}{RT} + \log\left\{0.4363\left(\frac{T}{100}\right)^{3/2}\right\} + \log\left(1-e^{-225.79/T}\right)+14.96 \qquad (26)$$

The K_p value calculated from this formula and the $\log K_p$ curve are given in Table 1 and Fig. 7 respectively. Though P_a and P_m can be caulculated from

Table 1. K_p (in mm Hg)

T	$\log_e K_p$	K_p
520	−1.397	0.2473
540	−0.745	0.4747
560	−0.139	0.8702
580	+0.425	1.5296
600	0.958	2.6065
620	1.462	4.3146
640	1.922	6.8346
660	2.363	10.623
680	2.771	15.975
700	3.160	23.570
720	3.528	34.056
740	3.878	48.328
760	4.216	67.762
780	4.520	91.836
800	4.828	124.96

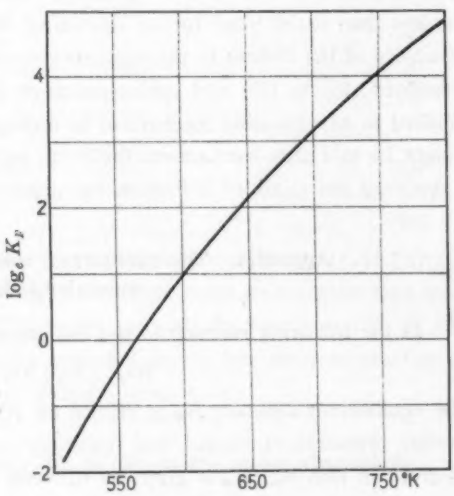

Fig. 7

K_p and the observed total pressure, this has not been done because it has already been performed by R. W. Ditchburn and J. C. Gilmour[15] using Kirchhoff's equation. The values of P_a and P_m obtained by them are shown in Fig. 8.

13) R. Ladenburg and F. Thiele: Zeits. f. Phys. Chem., **7** (1930) 161.
14) G. Herzberg: Molecular Spectra and Molecular Structure I.
15) R. W. Ditchburn and J. C. Gilmour: Rev. Mod. Phys., **13** (1941) 310.

If the temperature increases under the condition that sodium exists only in the gas phase, P_a and P_m will vary according to K_p, and molecular sodium will dissociate into the atomic sodium. In the range of temperature 250°~300°C, P_m is only about 1/100 of P_a as seen in Fig. 8, and threfore the effect of the dissociated atoms on P_a can be neglected. The temperature derivative of the second and third terms of the above formula (26) can be neglected in comparison with the first term, so that the derivative of K_p is given by the following formula

$$\frac{\Delta \log K_p}{\Delta 1/T} = \frac{\log P_{m_0} - \log P_m}{1/T - 1/T_0} = -\frac{D}{R} . \qquad (27)$$

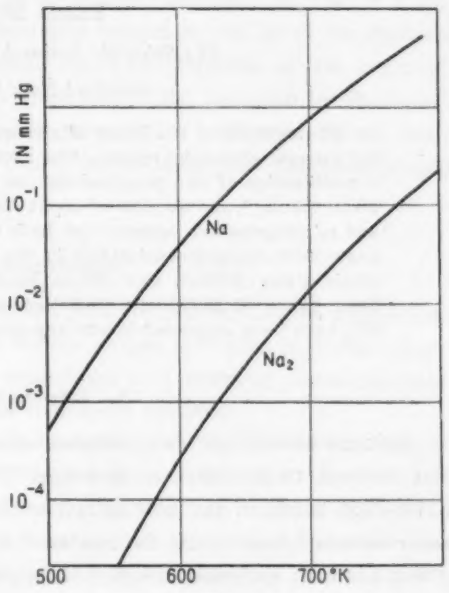

Fig. 8

The author wishes to express his sincere thanks to Professor D. R. Bates for his suggestions regarding the present work and to Professor Yoshio Fujioka, Director of the Institute, for his deep interest and valuable discussions. He is also much indebted to Professor Yoshio Tanaka for his encouragement and valuable advice during the course of this work and to Professor Haruo Ootsuka for his valuable discussion upon this work.

The Absorption Spectrum of Nitrogen Dioxide in the Vacuum Ultraviolet

Kazuo MORI

The Scientific Research Institute, Ltd.

(Received Nov. 18, 1953)

Photographs of the bands of nitrogen dioxide have been taken in the vacuum ultraviolet region. The λ 1600–1350 bands were arranged in a combination of two progressions, one with a frequency separation of about 600 cm^{-1}, and another of about 400 cm^{-1}. The relatively long ν_1' and ν_2' progressions indicate that both the bond distance and the apex angle have changed considerably in the transition to the excited electronic state. Fifteen new diffuse bands have been observed around λ 1800. Some of Mulliken's predictions on the electronic structure of NO_2 have been supported in our arguments.

1. Introduction

Nitrogen dioxide has many complicated absorption bands extending from the near infrared to the extreme ultraviolet[1)-6)]. The vibrational structure of the λ 2700–2300 bands in the near ultraviolet has been discussed on a considerably well established basis[5)], and the rotational structure of the λ 2491 band[7)] in this system has been analysed, though not completely, resulting in accurate information concerning the form and the fundamental frequencies of the NO_2 molecule both in the ground and in the excited electronic states. However, in most of the other regions, the bands are so diffuse and, even where relatively sharp, so irregulary arranged, that their vibrational analysis is hardly possible, except for the absorption bands in the vacuum ultraviolet, measured by Price and Simpson[6)], who proposed an analysis of the λ 1600–1350 system as a single progression.

In the past, during the study of the absorption spectra of nitric oxide[8)] in the vacuum ultraviolet, we have photographed the absorption spectra of NO_2 as

1) J. Curry and G. Herzberg: Nature, **131** (1933) 842.
2) J. K. Dixon: J. Chem. Phys., **8** (1940) 157.
3) T. C. Hall and F. E. Blacet: J. Chem. Phys., **20** (1952) 1745.
4) P. M. Lambrey: Compt. rend., **188** (1929) 251; Ann. de Phys., (10) **14** (1930) 95.
5) L. Harris, G. W. King, W. S. Benedict and R. W. Pearse: J. Chem. Phys., **8** (1940) 765.
6) W. C. Price and D. M. Simpson: Trans. Faraday Soc., **37** (1941) 106.
7) L. Harris and G. W. King: J. Chem. Phys., **8** (1940) 775.
8) Y. Tanaka, M. Seya and K. Mori: J. Chem. Phys., **19** (1951) 979 (L); Science of Light, **1** (1951) 80.

a possible impurity in the absorbing gas. We obtained spectra similar to those observed by Price, whose vibrational analysis of the λ 1600–1350 system seemed to be doubtful. Recently we measured them again, and upon reexamination of their vibrational structure, we arrived at an analysis different from that of Price. Referring to the data of the above-mentioned system as well as of the Rydberg series observed below λ 1300, we made some considerations on the electronic states of NO_2, and reached conclusions which support the prediction by Mulliken[9]. Moreover, from measurements at higher pressures, a number of diffuse bands not previously reported were found, hidden in the background continuum around λ 1800.

2. Experiment

NO_2, obtained by heating lead nitrate, was distilled fractionally several times by cooling with liquid air, in order to remove oxygen and other impurities generated at the same time. Storing the sample gas in a reservoir containing phosphoric oxide, water vapor was almost completely removed.

Photographs were taken with a one-meter normal incidence vacuum spectrograph having a dispersion of about 17 A/mm at the first order. The source of light was a Lyman discharge tube and the spectrograph chamber was used as absorption cell. The pressure of the absorbing gas in the chamber was varied from a thousandth to several tenths of a mm Hg depending on the extent of absorption in a given wavelength region. In most of the experiments we used no window at the slit of the spectrograph. At lower pressures, below 1/100 mm Hg, which are too low for the discharge to occur, hydrogen gas was led as a conducting gas into the discharge tube, and a separate pumping system set up for the light source and the spectrograph chamber to prevent hydrogen from mixing in the sample gas. At higher pressures, above a few mm Hg, the discharge was again found to be weakened, so here we used as the light source a hydrogen discharge tube with a thin quartz window. Although the quartz window used transmits only up to λ 1500, it is adequate because at such a high pressure the region below λ 1700 actually merges into a strong continuous absorption. This high pressure experiment was made mainly for the observation of diffuse bands round λ 2000.

Taking into consideration the strong photodissociation of NO_2, the sample gas was led as fast as possible through the chamber in order to provide a continual supply of fresh gas for the optical path. However, the great intensity of

9) R. S. Mulliken: Rev. Mod. Phys., **14** (1942) 204.

the ultraviolet light coming from the light source still produced enough NO and O_2 by photo-dissociation to show their absorption spectra slightly in our spectrograms.

NO_2 has a strong absorption in the ultraviolet region, particulary below about λ 2000, where the superimposed continuous absorption, most of which may be attributed to N_2O_4[3], also becomes rapidly stronger with increase of pressure, so that we made the measurements mostly at pressures of several hundredths of a mm Hg or lower. The λ 1600–1350 band system becomes evident in its structure around a few hundredths of a mm Hg, and beyond this wavelength, as reported by Price and Simpson[6], there appears a strong Rydberg series, whose first member is distinct even at a thousandth of a mm Hg. The region beyond λ 1100 is strongly overshadowed with the background continuum and the absorption of the photodissociation products.

3. Results and Discussion

A. λ 1600–1300 band system.

Price and Simpson[6] investigated the absorption in this region and concluded that this system consisting of relatively sharp bands corresponded to a single (or at most two) electronic transitions, constituting one progression with a single vibration frequency of about 200 cm^{-1}, which was identified with the deformation frequency ν_2' in the upper electronic state. Therefore, they suggested that only the ONO angle changed in this transition, and that this change was considerably large because of the large extension of the progression and the asymmetric intensity distribution, being steep on the short wavelength side.

In our spectrograms, too, a frequency separation near 200 cm^{-1} is certainly conspicuous, but the intervals between the bands are too irregular for the adoption of such a simple progression as suggested by Price to be accepted. Careful examination of the arrangement of bands and of the intensity variation through bands, as indicated in Fig. 1, suggests that their structure may be explained satisfactorily by classifying them in a combination of two vibrational progressions, one of which has a frequency separation of about 600 cm^{-1}, another of about 400 cm^{-1} (Table 1). The former may be attributed to the symmetrical valence frequency, ν_1', and the latter to the deformation frequency, ν_2', in the upper electronic state. These values correspond well with the values of ν_1'', 1320 cm^{-1}, and ν_2'', 640 or 750 cm^{-1}, of NO_2 in the normal state[5][10][11]. The fact that the ν_1'

10) G. B. B. M. Sutherland and W. C. Penney: Proc. Roy. Soc., **A156** (1936) 678; M. K. Wilson and R. M. Badger: Phys. Rev., **76** (1949) 472(A).

11) G. E. Moore: J. O. S. A., **43** (1953) 1045.

progression appears to be somewhat longer than the ν_2' suggests that, though the change of the apex angle is large, the bond distances also change considerably in the transition to the excited electronic state. Accordingly it is considered that in this transition an electron present in a strongly bonding orbital jumps to an orbital which has a considerably antibonding nature and is sensitive of the change of the ONO angle.

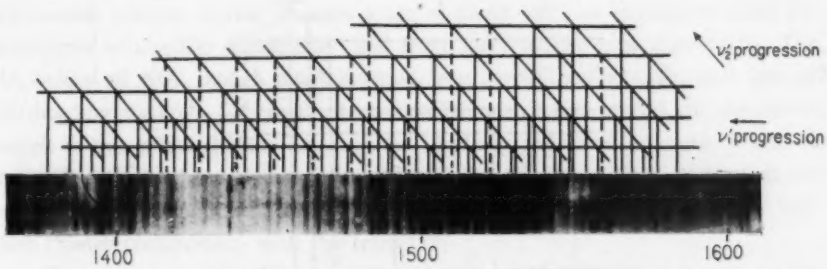

Fig. 1. A reproduction of the λ 1600–1350 absorption spectrum of NO_2, with a schematic representation of the vibrational analysis. The pressure of the absorbing gas was about 0.03 mm Hg. The path length of the absorbing column was 2 m. The photograph was taken by a 1 m normal incidence vacuum spectrograph. ν_1' is the symmetrical valence frequency, and ν_2' the deformation frequency in the excited electronic state. From considerations of the Franck-Condon principle, the vibrationless transition in this band system is expected to be very weak, and so the origin of this system would exist on the longer wavelength side of this region. In order to observe this band origin, measurements at higher pressures were required, but because of the overlapping of the continuous absorption in this range this was hardly possible.

Table 1. The λ 1600–1350 absorption band system of NO_2. Progressions in the longitudinal direction are those of ν_1' (symmetrical valence frequency), and those in the transverse direction of ν_2' (deformation frequency).

		63107	63492	63894
	63311	63715	64041	64466
63540	63939	64321	64642	65011
64135	64520	64901	65308	65651
64742	65138	65539	65876	66230
65355	65733	66194	66423	66814
65954	66326	66720	67065	67458
66551	66903	67277	67673	68064
67137	67508	67824	68241	68658
67732	68176	68549	68885	69247
68334	68757	69152	69565	69955
68937	69343	69735	70126	70517
69565	69955	70323	70666	
70126	70517	70917		
70746	71139	71521		
71342	71736	72108		

Fig. 2 represents an energy level diagram, suggested by Mulliken[9] for interpreting the relations between the electronic states and the absorption spectra of NO_2, and supplemented by us. In this diagram, the outer molecular orbitals of NO_2, occupied and unoccupied, are arranged according to the magnitude of the

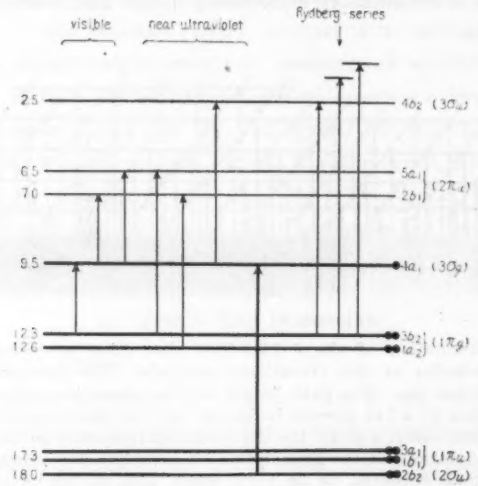

Fig. 2. The energy level diagram giving an interpretation of the NO_2 spectrum. (Cf. Mulliken 11) The column on the right designates the molecular orbital having the C_{2v} symmetry, the symbol in parenthis referring to the orbital having the $D_{\infty h}$ symmetry. The column on the left gives the ionization energy of each orbital in electron volts. Arrows indicate the observed transitions.

ionization energy. From the lower levels, pairs of electrons are filled in each orbitals up to the $3b_2$, when the total number of outer electrons is 16. In the linear triatomic molecules this number of outer electrons corresponds to the case of CO_2 or CS_2, whose electronic structure in the normal state consists of a set of firmly bound closed shells of electrons, giving a chemically saturated structure, like the rare gas. NO_2 has 17 outer electrons, one more than those of CO_2, the last one of which has to go into orbitals above the $3b_2$. It is expected, reasoning from the case of CO_2^+, that orbitals below $3b_2$ have a bonding or nonbonding nature and those above $3b_2$ an antibonding nature. This situation is closely analogous to that which is met in the diatomic molecule, NO. The normal state of NO is... $\ldots(\pi_u 2p)^4\ \pi_g 2p,\ ^2\Pi_g$[12]. In addition to the stable closed shell,$\ldots\ldots(\pi_u 2p)^4$, of N_2 or CO, NO has one more electron in an antibonding $\pi_g 2p$ orbital, so that the

12) G. Herzberg: Molecular Spectra and Molecular Structure, I (1950), 343.

molecule of NO is less stable than that of N_2 or CO. Similarly, the last electron of NO_2 entering into an antibonding and high energy orbital should make the NO_2 molecule much more unstable than that of CO_2 or CS_2.

However, unlike the case of the diatomic molecule, the triatomic molecule is able to change the state of symmetry by an alteration in the shape of the molecule, the energy of the antibonding orbital thus being somewhat lowered, and the molecule a little stabilized. Actually, the shape of NO_2 molecule is known to be an isoscele triangle having an apex angle of about 130°, as established from experiments of electron diffraction[13] and from spectroscopic measurements[9]. The $4a_1$ orbital of NO_2, though much lowered, may be still rather high, and has an antibonding nature[9]. If, in the transition from an inside orbital, an electron is added to this orbital having an unpaired electron, the bond strength would be reduced and the bond distance lengthened. At the same time, because of the sensitiveness of this orbital to the change of apex angle, the ONO angle may also change considerably with the transition.

The maximum absorption intensity for the λ 1600–1350 system is near λ 1450, which corresponds to an excitation energy of about 8.5 eV. As will be seen later, the nonbonding $3b_2$ or $1a_2$ orbital corresponding to the $1\pi_g$ orbital of CO_2 may have an ionization potential of about 13 eV or somewhat smaller, and a band belonging to a transition of about 8.5 eV from these orbitals should be ascribed to a member of the Rydberg series converging to the second ionization potential. Furthermore, from higher orbitals than these nonbonding orbitals, no transition having a similar order of energy is possible. Thus, the transition from orbitals inside should be considered. Next to the nonbonding orbitals are the $3b_1$, $1b_1$ orbital ($1\pi_u$) or the $2b_2$ orbital ($2\sigma_u$), all of which are the constituents of double bonds between the N and O atoms. With reference to the data of the Rydberg series of CO_2[14], they may be considered to have ionization potentials around 18 eV. When an electron transits from one of these orbitals with an excitation energy of about 8.5 eV, it is expected to arrive at an orbital having an ionization energy of about 9.5 eV. This value agrees well with that of the $4a_1$ orbital, which was given to account for the absorption spectra of NO_2 in the visible and near ultraviolet (cf. Fig. 2). In conclusion, the λ 1600–1350 system may be considered to correspond to the transition ($3a_1$, $1b_1$ or $2b_2$)$\rightarrow 4a_1$.

On the other hand, the total intensity of this absorption band system is very large and comparable to that of the neighbouring Rydberg series. This fact

13) Clasesson, Donohue and Schomaker: J. Chem. Phys., **16** (1948) 207.

14) H. J. Henning: Ann. d. Physik, (5) **13** (1932) 599; G. Rathenau: Zeits. f. Physik, **87** (1933) 32.

suggests immediately that the λ 1600–1350 system is due to the transition of the $N \rightarrow V$ type[15], as Price and Simpson have remarked. This also supports the above-mentioned interpretation of the band system as belonging to the bonding→ antibonding transition.

Whether this transition is of the $\sigma_u \rightarrow \sigma_g$ type (that is $2b_2 \rightarrow 4a_1$) or the $\pi_u \rightarrow \sigma_g$ type (that is $3a_1$, $1b_2 \rightarrow 4a_1$) could not be decided[16] until, the shape of the band envelope is made clearer by photographing under high dispersion, and, if possible, the distinction is made of whether the type is of the parallel or the perpendicular, even though the rotational analysis of these bands may be impossible. However, from the fact that in our plates each band seems to shade off slightly towards the red and that the ν_1' and ν_2' progressions have different lengths, it appears to be rather probable that the λ 1600–1350 system belongs to the $2b_2 \rightarrow 4a_1$ transition of parallel type.

In this λ 1600–1350 band system, there seems to be a predissociation around λ 1480 (about 8.5 eV), although this is not very certain. If this is the case, it is probable that the dissociation products are NO ($A^2\Sigma$) and O(^3P), because it is known that the energy required for the transition of NO from the ground state to the upper state of the γ bands ($A^2\Sigma$ state) is 5.3 eV, and that the first predissociation[17] of NO_2 around λ 3700 (3.3 eV) produces NO ($^2\Pi$, the ground state) and O(^3P).

B. Rydberg series and the first ionization potential[18].

In the region below λ 1300 there appears a Rydberg series, as Price and Simpson have reported. Although the position of its first member is distinct and does not have room for doubt, that of the second member is uncertain on account of the background continuum and the absorption of impurities produced by photodissociation. Our previous tentative selection of members of the Rydberg series was different from that of Price, but, in every case, the value of 12.5–13.0 eV may be obtained as the ionization potential. This Rydberg series converging to the second ionization potential is certainly due to the transition of a nonbonding π electron ($3b_2$ or $1a_2$) localized at the oxygen atom.

As regards the ionization potential of 11 eV observed in the electron impact

15) R. S. Mulliken: J. Chem. Phys., **7** (1939) 20.

16) N. Metropolis: Phys. Rev., **60** (1941) 283.

17) R. G. W. Norrish: J. Chem. Soc., (1929) 1158.

18) If Price's Rydberg series formula $\nu_0^n = 99500 - \frac{R}{(n+0.25)^2} (n=2, 3, \ldots)$ is correct, the bands of the third member are tentatively chosed in our plates as follows

A	cm^{-1}	A	cm^{-1}
1085	92166	1070	93458
1078	92764	1064	93985

experiment[19], though the accuracy of the electron impact measurement is doubtful, our foregoing arguments seem to support Mulliken's prediction[20] that it corresponds to the removal of an odd electron from the $4a_1$ orbital, and that therefore this value corresponds to the first ionization potential of NO_2. Contrary to this prediction, Price and Simpson have suggested that the $4a_1$ level was actually much lowered and had a more bonding nature, and that the first ionization potential of NO_2 might be that of an electron in the nonbonding orbital ($3b_2$ or $1a_2$). It is probably impossible to pick up members of the Rydberg series out of the overlapping strong bands, as in the case of NO. Recently, Watanabe et al[21] succeeded in observing the first ionization potentials of NO and of some other polyatomic molecules by means of an ingenious method. Their method will succeed also in observing the accurate first ionization potential of NO_2.

C. Diffuse bands around λ1800.

In the well-known λ 2700–2300 absorption band system in the near ultraviolet, there is a predissociation at λ 1459[9][17], beyond which bands become very diffuse and where the strong absorption of the background continuum begins. Lambrey[4] observed diffuse bands up to λ 2083, but in the present work many more bands, as shown in Table 2, have been detected. Since they appear rather inconspicuously, changing rapidly with wavelength, they are difficult to observe. Frequency intervals of about 930 cm^{-1} and 540 cm^{-1} are conspicuous in them. In this absorption range around λ 1800, there may be a band system corresponding to the $4a_1 \rightarrow 4b_2$ transition, as predicted by Mulliken (Fig. 2).

Table 2. New diffuse bands of NO_2 found in the range of λ 2050–1740. Wavelengths of bands are measured at about the centers.

A	cm^{-1}	A	cm^{-1}
2042	48972	1866	53591
2012	49702	1853	53967
1975	50633	1838	54407
1945	51414	1820	54945
1926	51921	1790 ?	55866
1906	52466	1771	56465
1891	52882	1743	57372
1876	53305		

The author wishes to express his sincere gratitude to Professor Y. Fujioka for his encouragement and guidance. Also he is much indebted to Dr. Y. Tanaka for his kind suggestions and advices.

19) E. C. G. Stueckelberg and H. P. Smith: Phys. Rev., **36** (1930) 478.
20) R. S. Mulliken: J. Chem. Phys., **3** (1935) 738.
21) K. Watanabe, E. F. Marmo and E. C. Y. Inn: Phys. Rev., **91** (1953), 1155; E. C. Y. Inn: Phys. Rev., **91** (1953) 1194.

The Ultraviolet Absorption Spectra of Formic Acid

YŌZŌ KAIFU

Institute of Polytechnics, Osaka City University

(Received February 1, 1954)

The ultraviolet absorption spectra of the formic acid in several solvents and its vapor phase have been investigated in the region λλ 2600~2100 A.

The solution spectrum in this region reveals almost no structure even in the less polar solvent, and the extinction coefficient increases rapidly from 2600 A to 2100 A.

The spectrum of the vapor shows considerable evidence of structures, and progressions of 1089, 825, 669, 482, 424, 368, 41 and 31 cm^{-1} are observed. The progression of 1089 cm^{-1} is assigned to a totally symmetrical C-O vibrational frequency in the excited state of the formic acid molecule.

1. Introduction

The ultraviolet absorption spectra of the formic acid have been studied by Price and Evans[1], who reported two absorption bands near 1550 A and in the λλ 1400~1100 A region. Another investigation has been made by Sugarman[2], who observed 22 diffuse bands between 2500 A and 2270 A. However, the analyses of these longer wavelength bands cannot be considered as yet complete.

In recent years, Ham and Platt[3] reported the ultraviolet absorption spectra of peptides, and discussed the $n \rightarrow \pi^*$ transition of the acid chromophore (–COOH) and the amide chromophore ($-CONH_2$). In view of these findings, it seems to be important to study the longer wavelength transition ($n \rightarrow \pi^*$ transition) of relatively simple molecules with –C=O, –COOH, $-CONH_2$ and similar groups.

A number of spectropic studies in the ultraviolet region have been published for simple aldehydes and ketones[4~7], but similar studies on simple fatty acids and their derivatives are not numerous. Based on these observations, the author

1) W. Price and W. N. Evans: Proc. Roy. Soc., **A 162** (1937) 110.
2) B. Sugarman: Proc. Phys. Soc., **55** (1943) 429.
3) G. S. Ham and J. R. Platt: J. Chem. Phys., **20** (1952) 335.
4) V. Henri and S. A. Schou: Zeit. f. Physik, **49** (1928) 774, S. A. Schou: J. Chim. Phys., **26** (1929) 665.
5) E. Eastwood and C. P. Snow: Proc. Roy. Soc., **A 149** (1935) 434.
6) G. Hertzberg: Tr. Farad. Soc., **27** (1931) 378.
7) E. J. Bowen and H. W. Thompson: Nature, **133** (1934) 571.

made an attempt to investigate the ultraviolet absorption spectra of the formic acid.

2. Experimental Procedure

The ultraviolet absorption spectra of liquid formic acid in a solvent of (a) *n*-hexane and ether mixture and (b) ethyl alcohol were studied with a Beckman quartz spectrograph.

The absorption spectrum of formic acid vapor was studied with a Hilger E_2-type spectrograph. The quartz absorption cell is 50 cm in length and has a side tube for reserve samples. An A.C. high voltage hydrogen discharge tube with water cooling (2000 V, 1 kW) was used for the light source.

Anhydrous formic acid was purified by drying with anhydrous boric acid and by vacuum distillation. To avoid dissociation and moisture, the pure anhydrous sample was sealed off in the absorption cell immediately upon preparation.

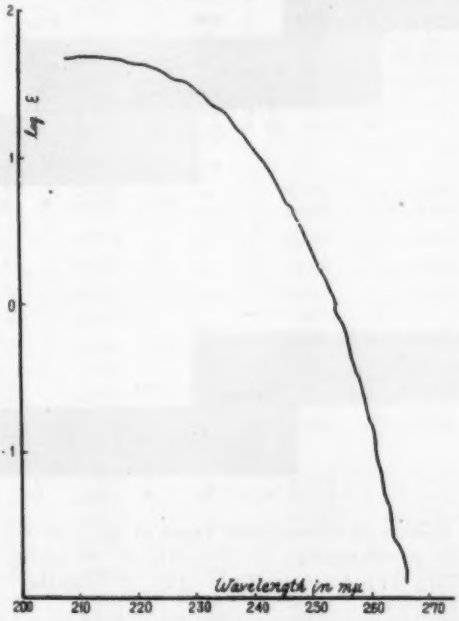

Fig. 1. Solution Spectrum of Formic Acid in n-hexane and Ether Mixture.

As is well known, double molecules dominate in the vapor of formic acid at room temperature, and dissociate at temperatures above 150°C. To study absorption spectra of formic acid molecules both in the single and the double

states, the spectro-photographs were taken at ordinary temperature and at 200°C, while the reservoir temperature was adjusted between −20°C and 90°C for controlling the vapor pressure.

3. Experimental Results

The absorption curve of liquid formic acid in the *n*-hexane and ether solvent is plotted in Fig. 1. The absorption begins at about 2650 A, the extinction coefficient increasing rapidly towards the shorter wavelength regions. The maximum absorption peak was found to occur at about 2120 A and its molar extinction coefficient to be 47.4. With the ethyl alcohol solution, the absorption curve was much smoother, but the band positions were almost identical.

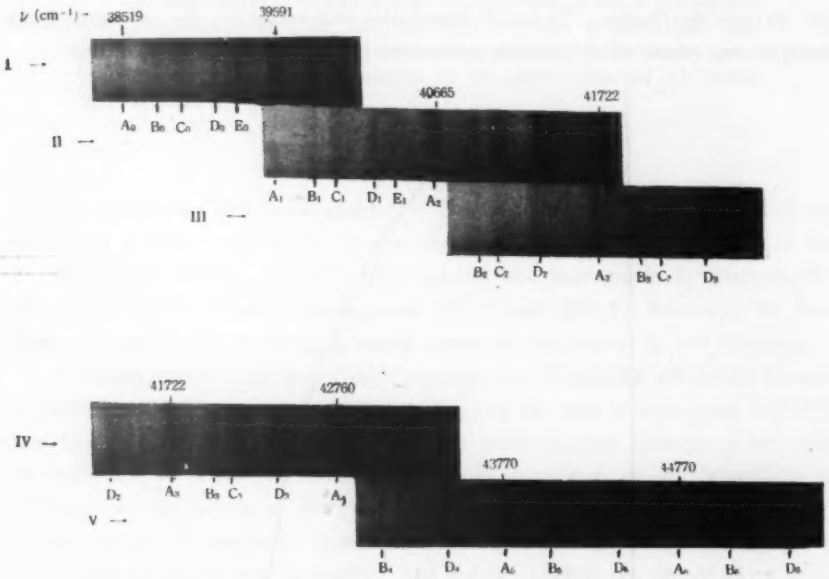

Fig. 2. Spectra of Formic Acid Vapor at 200°C in 50 cm cell.
(I) p=500 mmHg (II) p=100 mmHg
(III), (IV) p=50 mmHg (V) p=8 mmHg.

About 80 bands were observed between 2600 A and 2200 A in the vapor absorption spectrum of the formic acid, as shown in Fig. 2 and Table I. The bands became gradually intense and diffuse towards the shorter wavelength region, and below 2180 A the absorption became continuous at least as short as far down 1900 A. This may be interpreted to be due to the predissociation of

Table I. Absorption Bands of Formic Acid.

Series Assignment	Wavelength (A)	Wavenumber (cm^{-1})	Intensity	Calcu. Wavenumber	Assignment
A_0	2597.6	38485	vw	38478	e−41
	2595.3	38519	vw	—	e
	2584.5	38680	ew		
B_0	2579.9	38749	vw	38754	e+235
	2577.8	38781	vw	38785	e+235+31
	2576.1	38806	ew		
C_0	2567.2	38941	vw	38943	e+424
	2563.6	38995	ew	39001	e+482
	2557.5	39088	ew		
D_0	2553.8	39145	vw	39147	e+669−41
	2551.4	39182	vw	39188	e+669
	2546.1	39263	ew		
	2544.5	39288	ew		
E_0	2542.9	39313	vw		
	2540.9	39344	vw	39344	e+825
A_1	2526.6	39566	w	39560	e+(1089−7)−41
	2525.0	39591	w	39601	e+(1089−7)
	2523.0	39623	vw	39632	e+(1089−7)+31
	2520.8	39657	ew		
	2517.7	39706	ew		
	2513.8	39768	ew		
B_1	2510.7	39818	w	39836	e+(1089−7)+235
	2508.4	39854	w	39867	e+(1089−7)+235+31
C_1	2500.9	39973	w	39969	e+(1089−7)+368
C_1'	2498.0	40019	w	40025	e+(1089−7)+424
	2493.9	40085	ew	40083	e+(1089−7)+482
	2492.5	40107	ew		
D_1	2485.0	40228	w	40229	e+(1089−7)+669−41
	2482.7	40266	w	40270	e+(1089−7)+669
	2475.2	40388	w		
E_1	2472.6	40430	w	40426	e+(1089−7)+825
	2470.5	40465	vw		
A_2	2460.8	40623	m	40628	e+(1089×2−7×4)−41
	2458.4	40665	m	40669	e+(1089×2−7×4)
	2456.7	40693	w	40700	e+(1089×2−7×4)+31
	2453.1	40752	vw		
	2450.6	40794	vw		
B_2	2444.0	40904	m	40904	e+(1089×2−7×4)+235
	2442.4	40931	m	40935	e+(1089×2−7×4)+235+31
C_2	2436.4	41032	m	41037	e+(1089×2−7×4)+368
C_2'	2432.8	41092	m	41093	e+(1089×2−7×4)+424
	2429.3	41152	vw	41151	e+(1089×2−7×4)+482
D_2	2420.9	41294	m	41297	e+(1089×2−7×4)+669−41
	2418.5	41335	m	41338	e+(1089×2−7×4)+669

Table I. (Continued)

Series Assignment	Wavelength (Å)	Wavenumber (cm^{-1})	Intensity	Calcu. Wavenumber	Assignment
	2413.1	41428	m		
E_2	2409.1	41497	m	41494	e+(1089×2−7×4)+825
A_3	2398.6	41678	m	41682	e+(1089×3−7×9)−41
	2396.1	41722	m	41723	e+(1089×3−7×9)
	2394.2	41755	w	41754	e+(1089×3−7×9)+31
	2390.1	41826	w		
B_3	2382.5	41960	s	41958	e+(1089×3−7×9)+235
	2380.2	42000	s	41989	e+(1089×3−7×9)+235+31
C_3	2375.4	42085	m	42091	e+(1089×3−7×9)+368
C_3'	2371.7	42151	m	42147	e+(1089×3−7×9)+424
	2368.4	42210	w	42205	e+(1089×3−7×9)+482
D_3	2360.0	42360	s,d	42351	e+(1089×3−7×9)+669−41
	2353.7	42473	m		
E_3	2350.0	42540	m	42548	e+(1089×3−7×9)+825
	2345.5	42622	w		
A_4	2340.2	42718	s	42722	e+(1089×4−7×16)−41
	2337.9	42760	s	42763	e+(1089×4−7×16)
	2336.0	42795	m	42794	e+(1089×4−7×16)+31
	2335.3	42808	w		
	2332.6	42858	w		
B_4	2324.5	43007	vs,d	42998	e+(1089×4−7×16)+235
	2322.9	43036	vs,d	43029	e+(1089×4−7×16)+235+31
C_4	2317.4	43139	s	43131	e+(1089×4−7×16)+368
C_4'	2314.5	43193	m	43187	e+(1089×4−7×16)+424
D_4	2303.7	43395	vs,d	43391	e+(1089×4−7×16)+669−41
	2301.1	43444	vs,d	43432	e+(1089×4−7×16)+669
	2296.2	43537	s,d		
A_5	2284	43770	vs,d	43789	e+(1089×5−7×25)
B_5	2270	44040	vs,b	44024	e+(1089×5−7×25)+235
C_5	2262	44190	vs,b	44213	e+(1089×5−7×25)+424
D_5	2249	44450	vs,b	44458	e+(1089×5−7×25)+669
A_6	2233	44770	vs,b	44806	e+(1089×6−7×36)
B_6	2219	45050	vs,b	45041	e+(1089×6−7×36)+235
C_6	2212	45190	vs,b	45230	e+(1089×6−7×36)+424
D_6	2199	45460	vs,b	45475	e+(1089×6−7×36)+669

the molecule.

All bands measured are listed in Table I. The alphabetical notations found in the first column and also found in Fig. 2 represent the band series, the bands belonging to the same series being assigned the same letter. The second and the third columns respectively indicate the wavelengths and the corresponding

wavenumbers. The fourth column gives the intensity measured by visual estimation. Notations used in the column are as follows: ew—extremly weak, vw —very weak, w—weak, m—medium, s—strong, vs—very strong, d—diffuse and b—broad. Those marked b or d are accurate within 50 cm^{-1}, while the rest are accurate within 10 cm^{-1}.

4. Discussion

General Remarks on the Electronic Levels

In discussing the formic acid spectra. it is natural to compare them with the spectra of aldehydes or ketones. As a general rule the carbonyl group in a molecule produces a weak absorption band in the region of relatively long wavelengths. This absorption band always appears around 2900 A in saturated aldehydes and ketones, and possesses a relatively low intensity (molar extinction coefficient $\varepsilon=10\sim100$) which is of the same order of magnitude for all aldehydes and ketones.

As discussed by Mulliken[8] and McMurry[9], these long wavelength transitions in aldehydes and ketones may be attributed to the excitation of a nonbonding electron localized on the oxygen atom to the excited π-molecular orbitals of the C=O group,—designated $^1A—^1U$ transition ($n\rightarrow\pi^*$ transition) according to the Platt's notation[10].

In the formaldehyde, this transition occurs between 3700 A and 2500 A[4], and obviously the absorption band of the formic acid mentioned above corresponds to this $^1A—^1U$ transition, as discussed by McMurry[11]. As mentioned in the previous section, this band extends from 2600 A to about 1900 A. So, comparing the two molecules formaldehyde $\begin{matrix}H\\H\end{matrix}\!\!>\!C=O$ and formic acid $\begin{matrix}H\\HO\end{matrix}\!\!>\!C=O$, the $^1A—^1U$ transition band may thus be said to shift about 1000 A towards the shorter wavelength side with the substitution of the OH group for the hydrogen. An analogous relationship may be recognized between formaldehyde, acetaldehyde $\begin{matrix}CH_3\\H\end{matrix}\!\!>\!C=O$, and propionaldehyde $\begin{matrix}C_2H_5\\H\end{matrix}\!\!>\!C=O$, the absorption bands of which

8) R. S. Mulliken: J. Chem. Phys., **3** (1935) 564.
9) H. L. McMurry: J. Chem. Phys., **9** (1941) 231.
10) J. R. Platt: J. Opt. Soc. Am., **43** (1953) 252.
11) H. L. McMurry: J. Chem. Phys., **10** (1942) 655.

begin at 3700 A, 3400 A and 3370 A, respectively[12]. This again is an example of the $n \rightarrow \pi^*$ transition band shifting toward the shorter wavelength side by substitution. On the contrary, the $\pi - \pi^*$ transition bands in conjugated systems shift towards the longer wavelength side by substitution, as in well known in the case of benzene[13),14)] and ethlene[13)] and their derivatives.

Since in the case of *p*-benzoquinone, toluquinone and *p*-xyloquinone the band maxima occur at 4465 A, 4425 A and 4350 A respectively, the above substitution effect for the $n \rightarrow \pi^*$ transition may also be found in aromatic aldehydes and ketones. This blue shift of the $n \rightarrow \pi^*$ band may be considered to parallel the correlation between the polarity of the –C—O bond and the ionization potential of the oxygen nonbonding electrons, as discussed by Walsh[15)]. Also, this substitution effect is parallel qualitatively to the solvent effect of the $n \rightarrow \pi^*$ transition discussed by McConnel[16)]. Further investigation of these effects for relatively simple molecules is now being undertaken and details will be reported in the future.

Analysis of the Spectra

There are five band series which have been observed to be prominent, and these have been designated A, B, C, D and E in Fig. 2 and Table I. All of these might most logically be attributed to transitions from the lowest vibrational level of the ground state to the upper state. In each of these series the bands are spaced about 1089 cm^{-1} apart. These features of the formic acid spectra are closely analogous to that of the formaldehyde spectra analyzed by Henri and Schou[4)], and Hertzberg[6)]. The absorption bands of formaldehyde have a characteristic spacing of 1180 cm^{-1}. This has been interpreted as a totally symmetrical C—O vibration in the excited state, as also the progression of 1089 cm^{-1} observed in formic acid spectra. Furthermore, this interpretation is suported by the occurrence of a similar vibrational frequency of 1050 cm^{-1} found in the excited state of the acetaldehyde and other aldehydes[5)].

As in the formaldehyde, the progression of 1089 cm^{-1} decreases systematically towards shorter wavelengths. The mean differences between successive groups: (A_0, B_0, C_0, D_0, E_0) and (A_1, B_1, C_1, D_1, E_1); (A_1, B_1, C_1, D_1, E_1) and (A_2, B_2, C_2, D_2, E_2); (A_2, B_2, C_2, D_2, E_2) and (A_3, B_3, C_3, D_3, E_3); (A_3, B_3, C_3,

12) R. W. B. Pearse and A. G. Gaydon: "*The Identification of Molecular Spectra*" John Wiley & Sons Inc. (1950) New York.
13) J. R. Platt: J. Chem. Phys., **19** (1951) 101.
14) W. W. Robertson and F. A. Matson: J. Am. Chem. Soc., **72** (1950) 5252.
15) C. A. Coulson: "*Valence*" p. 185,
16) H. McConnell: J. Chem. Phys., **20** (1952) 700.

D_3, E_3) and (A_4, B_4, C_4, D_4, E_4) are 1083 cm^{-1}, 1069 cm^{-1}, 1059 cm^{-1}, and 1042 cm^{-1}, respectively. This systematic diminution may be attributed to the anharmonicity of the molecular vibration.

If the first member of the A-series (A_0=38519 cm^{-1}) is considered to arise from the (O, O)-transition, the following formula will enable us to calculate all the bands of the A-series, which should provide satisfactory agreement with the observed frequencies if our surmise is correct.

$$\nu = 38519 + 1089\,v - 7\,v^2, \quad v = 0, 1, 2, \ldots .6$$

Similarly, the other band series may be interpreted to conform to the following formulae:

B-series

$$\nu = 38519 + 1089\,v - 7\,v^2 + 235$$
$$\nu = 38519 + 1089\,v - 7\,v^2 + 235 + 31$$

C-series

$$\nu = 38519 + 1089\,v - 7\,v^2 + 424$$
$$\nu = 38519 + 1089\,v - 7\,v^2 + 482$$

D-series

$$\nu = 38519 + 1089\,v - 7\,v^2 + 669 - 41$$
$$\nu = 38519 + 1089\,v - 7\,v^2 + 669$$

E-series

$$\nu = 38519 + 1089\,v - 7\,v^2 + 825$$

The assignments and calculated wavenumbers are found in Table I, but they are not entirely accurate, since some of these band progressions are not constant and decrease more or less systematically towards shorter wavelength regions. For more accurate assignment, however, it may be necessary to perform measurements with under higher dispersion.

The formic acid molecule is plane and has the symmetry C_s. Of the nine fundamentals, seven are vibrations in the plane of the molecule and two are perpendicular to it[17]. As Raman and infrared data available at present are not adequate, it is difficult to make a detailed discussion of the above band progressions and the molecular vibrational frequencies obtained by the Raman and infrared measurements. The main progression of 1089 cm^{-1}, assigned to the totally symmetrical C—O vibration of the excited state, might correspond to a ground state frequency of 1093 cm^{-1} which is assigned to the planer frequency of H—C(=O)—O vibration[18]. Another progression of 669 cm^{-1} might correspond

17) G. Hertzberg: "*Molecular Spectra and Molecular Structure*" II Infrared and Raman Spectra of Polyatomic Molecules p. 322.

18) I. G. Bonner and R. Hofstadter: J. Chem. Phys., **6** (1938) 531, R. Hofstadter: J. Chem. Phys., **6** (1938) 540.

to the perpendicular frequency of 698 cm^{-1} in the ground state[19].

The spectra of the formic acid were also investigated at two temperatures, corresponding to the single and double molecules, but their appearance did not change noticeably.

Acknowledgment

The author wishes to express his gratitude to Professor Okuda for his kind instructions, and to Mr. Hanawa for his helpful suggestions.

19) B. D. Saksena: Proc. Ind. Acad. Sci., **A 12** (1940) 312.